Hindawi
Shock and Vibration
Volume 2019, Article ID 9234832, 21 pages
https://doi.org/10.1155/2019/9234832

Research Article

Theoretical and Numerical Studies on Damped Nonlinear Vibration of Orthotropic Saddle Membrane Structures Excited by Hailstone Impact Load

Changjiang Liu[1,2] **Fan Wang**[3] **Jian Liu**[1,2] **Xiaowei Deng**[4] **Zuoliang Zhang**[3] **and Haibing Xie**[3]

[1]*School of Civil Engineering, Guangzhou University, Guangzhou 510006, China*
[2]*Guangdong Engineering Technology Research Center for Complex Steel Structures, Guangzhou University, Guangzhou 510006, China*
[3]*College of Environment and Civil Engineering, Chengdu University of Technology, Chengdu 610059, China*
[4]*Department of Civil Engineering, The University of Hong Kong, Pokfulam, Hong Kong 999077, China*

Correspondence should be addressed to Changjiang Liu; changjiangliucd@126.com, Fan Wang; warmfun@126.com, Jian Liu; liuj5000@163.com, and Xiaowei Deng; xwdeng@hku.hk

Received 25 February 2019; Accepted 28 May 2019; Published 24 July 2019

Academic Editor: Davood Younesian

The orthotropic membrane structures have been popular in architectural structures. However, because of its lightweight and small stiffness, large nonlinear deflection vibration may occur under impact load, which leads to structural failure. In this paper, the governing equations of the large deflection nonlinear damped vibration of orthotropic saddle membrane structures excited by hailstone impact load are proposed according to the von Kármán's large deflection theory and solved by applying the Bubnov–Galerkin method and the method of KBM perturbation. The approximate theoretical solution of the frequency function and displacement function of the large deflection nonlinear damped vibration of saddle membrane structures with four edges fixed excited by hailstone impact was obtained. The analytical examples proved that the mode shape function (equation (43)) can be applied to calculate the single-order mode shapes and the total superposed mode shapes of the damped large nonlinear deflection vibration of orthotropic saddle membrane structures excited by hailstone impact load succinctly. In addition, we compare and analyze the results of vibration frequency, amplitude, time histories, and total displacement of membrane structures with different pretensions and arch-to-span ratios under the impact of differently sized hailstones. The correctness of the analytical theory is verified by comparing with the results of numerical simulation. According to the results of this paper, we put forward some suggestions for the vibration control and dynamic design of practical spatial membrane structures.

1. Introduction

The membrane structure which is made of orthotropic membrane materials has been popular in architectural structures, and the saddle membrane structure is one of the most common shapes of the double-curved membrane [1, 2]. However, because of its lightweight, large flexibility, and small stiffness, it is very sensitive to impact load. Large nonlinear deflection vibration occurs under impact load, which may lead to structural failure [3, 4]. Thus, it is necessary to study damped large nonlinear deflection vibration of orthotropic saddle membrane structures excited by hailstone impact load.

In recent decades, more and more attention has been focused on the dynamic characteristics of the membrane. By applying the Hamilton principle and Galerkin method, Shin et al. [5, 6] obtained the natural frequencies and mode shapes of the free vibration for an axially moving membrane. The results showed that the translating speed, aspect ratio, and boundary conditions have significant effects on the in-plane vibrations of the moving membrane. Pan and Gu [7] adopted D'Alembert's principle to deduce the free oscillating

system's equivalent fundamental frequency of the square tensioned membrane. The effects of prestrain, size, elastic ratio, density, relative amplitude, and dead load on the nonlinearity of square pretensioned membrane were studied. Zheng et al. [8], Liu et al. [9], and Li et al. [10] investigated the large deflection nonlinear free vibration of orthotropic rectangular membrane structure by applying von Kármán's large amplitude theory, D'Alembert's principle, Bubnov–Galerkin approximate method, and Lindstedt–Poincaré perturbation method and obtained the approximate analytical solution in power series of the nonlinear vibration frequency function and the displacement function of the rectangular membrane with four edges fixed. However, they only studied the free vibration of planar rectangular membrane structures.

On the basis of researches of the nonlinear free vibration of membrane structures, the investigations of the nonlinear forced vibration of membrane structures were performed. Gonçalves et al. [11] derived the equations of motion of the prestretched hyperelastic isotropic membrane with finite deformations and lateral pressure and obtained analytically the functions of natural frequencies and mode shapes of the membrane. The results show the stretching ratio significantly affected the linear and nonlinear vibrations of the membrane. Zheng et al. [12] applied D'Alembert's principle and the momentum theorem to derive the fundamental equations of forced vibrations of orthotropic membranes, which were solved according to the Lindstedt–Poincaré perturbation method, and obtained the formula of impact load and nonlinear forced vibration deflection of rectangular membranes with four edges fixed. However, the damping was not considered. By applying the Krylov–Bogolubov–Mitropolsky (KBM) perturbation method to solve the governing equations of large-amplitude nonlinear vibration of rectangular orthotropic membranes with viscous damping, Liu et al. [13] obtained the asymptotic analytical solutions for the frequency and displacement function of the planar rectangular membrane structure. However, the external load was not taken into consideration. According to the Föppl large deflection theory, Galerkin method, and multiple scale perturbation method, Zheng et al. [14] investigated the dynamic response of rectangular prestressed membrane subjected to concentrated impact load. Based on the von Kármán large deflection theory, D'Alembert's principle, the Bubnov–Galerkin method, and perturbation method, Liu et al. [15–17] studied nonlinear forced vibration of pretension rectangular orthotropic membrane structures with damping and without damping under single impact load. Based on the stochastic pulse theory and the random vibration theory, Zheng et al. [18] and Li et al. [19, 20] investigated the stochastic vibration problem of the orthotropic membrane subjected to random impact load through experimental and theoretical researches. Based on thin-plate theory and the Galerkin method, Li et al. [21] investigated the dynamic response of rectangular prestressed membrane subjected to uniform impact load theoretically and experimentally. The aforementioned studies, however, are limited to planar rectangular membrane structures.

On the current status, the studies on saddle membrane structure are concentrated on wind or rain loads. Yang and Liu [22] and Li and Sun [23] studied the aerodynamic critical unstable wind velocity of saddle membrane structure by applying the nonmoment theory and the potential flow theory. The aerodynamic interaction equations of the membrane structure were obtained and simplified by applying the Bubnov–Galerkin approximate method. By studying the free vibrations of membrane structures with the static and the dynamic effects of wind and snow, Lazzari et al. [24] analyzed the structural failure mechanisms of the roof of the Montreal Stadium membrane structure. Rizzo et al. [25] and Rizzo and Sepe [26] measured the pressure of the incoming wind on hyperbolic paraboloid roofs by conducting tests and finite element analyses. The possibility of defining equivalent static pressure fields able to reproduce the envelope of dynamic displacements of the cables net was explored. Wu et al. [27] studied the aeroelastic instability mechanism of a tensioned membrane structure. The response and wind velocities above two closed-type saddle-shaped tensioned membrane structures, with the different pretension levels, were measured in uniform flow and analyzed. The results indicate that the aeroelastic instability is caused by vortex-induced resonance. Xu et al. [28, 29] and Liu et al. [30] studied nonlinear wind-induced aerodynamic stability of orthotropic saddle membrane structures by establishing the interaction governing equations of wind-structure coupling based on von Kármán's large amplitude theory and D'Alembert's principle. They determined the critical velocity of divergence instability, by judging the stability of the characteristic equation of the system. Cui et al. [31] applied the Eulerian–Eulerian model according to multiphase flow theory, and the saddle membrane structure response analysis under the simultaneous actions of wind and rain was conducted. The influences of changes in wind speed and rain intensity on the saddle-shaped membrane structure response were compared. There are no researches about the problem of saddle orthotropic membranes under impact load.

In this paper, the approximate formulas of hailstone terminal velocity were substituted into the governing equations of the large deflection nonlinear damped vibration of orthotropic saddle membrane structures excited by impact load. And, solving the governing equations by applying the Bubnov–Galerkin method and the method of KBM perturbation, the approximate theoretical solution of the frequency function and displacement function of the large deflection nonlinear damped vibration of saddle membrane structures with four edges fixed excited by hailstone impact was obtained. In analytical examples, the dynamic responses of saddle membrane structures with different pretension levels and arch-to-span ratios excited by the impact of different diametral hailstones were compared and analyzed separately. The correctness of the analytical theory is verified by comparing with the results of numerical simulation. In addition, the results of this paper can be applied in computation for the vibration control and dynamic design of practical spatial membrane structure under impact load.

2. Modeling of Saddle Membrane Structure

In this paper, we study a saddle, namely, hyperbolic paraboloid, membrane structure with four edges simply supported under an impact load. The theoretical model of saddle membrane structure is shown in Figure 1. The orthogonal axes x and y are the two different Young's modulus fiber directions of orthotropic saddle membrane structures. a and b, respectively, are the spans in x and y axes. N_{0x} and N_{0y}, respectively, denote the pretension in x and y axes. f_1 and f_2, respectively, are the midspan arch in x and y axes. The point O is the center of the plane xoy. The sphere H is a hailstone; v_0 denotes the velocity of the hailstone; (x_0, y_0) is the impact point on membrane surface.

The saddle membrane model can be represented by [29]

$$z_0(x,y) = \frac{f_2(x-(a/2))^2}{(a/2)^2} - \frac{f_1(y-(b/2))^2}{(b/2)^2}, \tag{1}$$

where z_0 denotes the initial surface function of saddle membrane structure.

According to equation (1), the two initial principal curvatures in x and y directions are

$$\begin{cases} k_{0x} = \dfrac{\partial^2 z_0}{\partial x^2} = \dfrac{8f_2}{a^2}, \\ \\ k_{0y} = \dfrac{\partial^2 z_0}{\partial y^2} = \dfrac{-8f_1}{b^2}. \end{cases} \tag{2}$$

With the action of the pretensions N_{0x} and N_{0y} [28], we can obtain

$$k_{0x}N_{0x} + k_{0y}N_{0y} = 0. \tag{3}$$

3. Dynamic Governing Equations

According to the von Kármán's large deflection theory and D'Alembert's principle, the compatible equation and dynamic motion equation of orthotropic saddle membrane structures are [28]

$$\begin{cases} \rho_0 \dfrac{\partial^2 w}{\partial t^2} + c\dfrac{\partial w}{\partial t} - (N_x + N_{0x})k_x - (N_y + N_{0y})k_y \\ \\ + 2N_{xy}k_{xy} = p(x,y,t) \dfrac{1}{E_1 h}\dfrac{\partial^2 N_x}{\partial y^2} + \dfrac{1}{E_2 h}\dfrac{\partial^2 N_y}{\partial x^2} \\ \\ - \dfrac{\mu_1}{E_1 h}\dfrac{\partial^2 N_x}{\partial x^2} - \dfrac{\mu_2}{E_2 h}\dfrac{\partial^2 N_y}{\partial y^2} - \dfrac{1}{Gh}\dfrac{\partial^2 N_{xy}}{\partial x \partial y}, \\ \\ = \left(\dfrac{\partial^2 w}{\partial x\, \partial y}\right)^2 - \dfrac{\partial^2 w}{\partial x^2}\dfrac{\partial^2 w}{\partial y^2} - \left(k_{0x}\dfrac{\partial^2 w}{\partial y^2} + k_{0y}\dfrac{\partial^2 w}{\partial x^2}\right), \end{cases} \tag{4}$$

where ρ_0 is the areal density of membrane; N_x and N_y, respectively, are the stress increments in x and y directions; N_{xy} is the shear stress; N_{0x} and N_{0y}, respectively, are the initial stress in x and y directions; $w = w(x,y,t)$ is the lateral deflection; h is the thickness of membrane; E_1 and E_2, respectively, are Young's modulus in x and y directions; G is the shear modulus; μ_1 and μ_2, respectively, are Poisson's ratio in x and y directions; k_x and k_y, respectively, are the two principal curvatures in x and y directions; k_{0x} and k_{0y}, respectively, are the two initial principal curvatures in x and y directions; c is the damping coefficient of structure; $p(x,y,t)$ is the impact load in z direction.

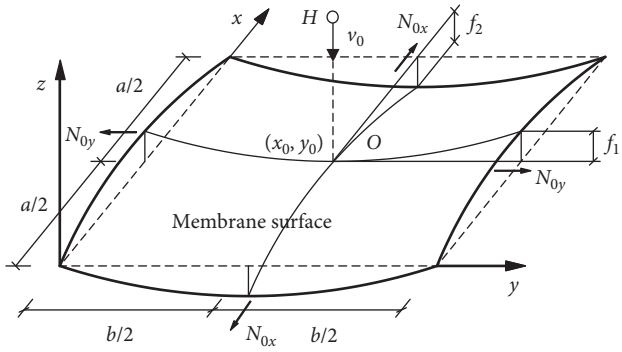

Figure 1: Pretensioned orthotropic saddle membrane model under an impact load with four edges simply supported.

According to the basic theory of plates and shells, the principal curvatures in x and y directions are [21]

$$\begin{cases} k_x = k_{0x} + \Delta k_x = k_{0x} + \dfrac{\partial^2 w}{\partial x^2}, \\ \\ k_y = k_{0y} + \Delta k_y = k_{0y} + \dfrac{\partial^2 w}{\partial y^2}, \end{cases} \tag{5}$$

where Δk_x and Δk_y denote the principal curvature increments in x and y directions, respectively.

By means of Airy's stress function $\varphi = \varphi(x,y,t)$, we can obtain [30]

$$\begin{cases} N_x = h\dfrac{\partial^2 \varphi}{\partial y^2}, \\ \\ N_y = h\dfrac{\partial^2 \varphi}{\partial x^2}, \\ \\ N_{xy} = -h\dfrac{\partial^2 \varphi}{\partial x\, \partial y}. \end{cases} \tag{6}$$

The effect of the shear stress is so small that we may assume that $N_{xy} = 0$. Therefore, according to equation (6), we can obtain

$$\frac{\partial^2 N_x}{\partial x^2} = \frac{\partial^2 N_y}{\partial y^2} = h\frac{\partial^4 \varphi}{\partial x^2 \partial y^2} = -\frac{\partial^2 N_{xy}}{\partial x\, \partial y} = 0. \tag{7}$$

By substituting equation (3) and equations (5)–(7) into equation (4), we can obtain

$$\rho_0 \frac{\partial^2 w}{\partial t^2} + c\frac{\partial w}{\partial t} - \left(h\frac{\partial^2 \varphi}{\partial y^2} + N_{0x}\right)\frac{\partial^2 w}{\partial x^2} - k_{0x}h\frac{\partial^2 \varphi}{\partial y^2} - \left(h\frac{\partial^2 \varphi}{\partial x^2} + N_{0y}\right)\frac{\partial^2 w}{\partial y^2} - k_{0y}h\frac{\partial^2 \varphi}{\partial x^2} = p(x, y, t), \tag{8}$$

$$\frac{1}{E_1}\frac{\partial^4 \varphi}{\partial y^4} + \frac{1}{E_2}\frac{\partial^4 \varphi}{\partial x^4} = \left(\frac{\partial^2 w}{\partial x\,\partial y}\right)^2 - \frac{\partial^2 w}{\partial x^2}\frac{\partial^2 w}{\partial y^2} - k_{0x}\frac{\partial^2 w}{\partial y^2} - k_{0y}\frac{\partial^2 w}{\partial x^2}. \tag{9}$$

Assume that the membrane does not bear an external load apart from the impact load; then, when the point of impact lies in the coordinates on (x_0, y_0) (as shown in Figure 1), the equation becomes [10]

$$p(x, y, t) = F(t)\delta\left((x - x_0)(y - y_0)\right), \tag{10}$$

where $F(t)$ is the impact force and $\delta(x, y)$ is the impulse function.

Assume that the initial displacement of the membrane is zero before the membrane is impacted by hailstone; when the hailstone is just in contact with the membrane, at the moment of $t = 0$, they have the same velocity, and this velocity is the initial velocity of the membrane, so the initial conditions are

$$w(x_0, y_0, t)\big|_{t=0} = 0, \qquad \left.\frac{\partial w(x_0, y_0, t)}{\partial t}\right|_{t=0} = v_0. \tag{11}$$

Impact loads are short-duration loads, so the maximum displacement amplitude $w_{\max}$ depends principally upon the magnitude of the applied impulse $I = \int_0^t F(\tau)d\tau$ and is not strongly influenced by the form of the load; thus, we can obtain the relational expression between $F(t)$ and $w(x, y, t)$ by the impulse theorem:

$$\int_0^t F(\tau)d\tau = Mv_0 - M\frac{\partial w(x_0, y_0, t)}{\partial t}, \tag{12}$$

where M is the mass of hailstone.

Derivation calculus to equation (12) yields

$$F(t) = -M\frac{\partial w^2(x_0, y_0, t)}{\partial t^2}. \tag{13}$$

Equations (8)–(13) are the fundamental equations applied in the analysis of saddle membrane excited by impact load.

According to the approximate formulas of hailstone terminal velocity [32], we can obtain the mass and velocity of hailstones (as shown in Table 1 and Figure 2).

The boundary conditions of the saddle membrane structure with four simply supported edges are

$$w|_{\text{at edges}} = 0, \qquad \left.\frac{\partial w^2}{\partial x^2}\right|_{\text{at edges}} = \left.\frac{\partial w^2}{\partial y^2}\right|_{\text{at edges}} = 0. \tag{14}$$

More concretely, the corresponding displacement and stress boundary conditions of every edges are

$$\begin{cases} w(0, y, t) = 0, \ \dfrac{\partial^2 w}{\partial x^2}(0, y, t) = 0, \\ w(a, y, t) = 0, \ \dfrac{\partial^2 w}{\partial x^2}(a, y, t) = 0, \end{cases} \qquad \begin{cases} w(x, 0, t) = 0, \ \dfrac{\partial^2 w}{\partial y^2}(x, 0, t) = 0, \\ w(x, b, t) = 0, \ \dfrac{\partial^2 w}{\partial y^2}(x, b, t) = 0, \end{cases} \tag{15}$$

$$\begin{cases} \dfrac{\partial^2 \varphi}{\partial x^2}(0, y, t) = 0, \\ \dfrac{\partial^2 \varphi}{\partial x^2}(a, y, t) = 0, \end{cases} \qquad \begin{cases} \dfrac{\partial^2 \varphi}{\partial y^2}(x, 0, t) = 0, \\ \dfrac{\partial^2 \varphi}{\partial y^2}(x, b, t) = 0. \end{cases} \tag{16}$$

4. Solution of Fundamental Equations

The functions that satisfy the displacement conditions of every edges equation (15) are separated as follows [12, 13]:

$$w(x, y, t) = \sum_{m,n} T_{mn}(t) \cdot W_{mn}(x, y), \tag{17}$$

where $W_{mn}(x, y)$ is the given deformation function; $T_{mn}(t)$ is the function of time; m and n are the positive integer.

According to the basic vibration theory and boundary conditions, the displacement function is given by

$$W(x, y) = \sin\frac{m\pi x}{a}\sin\frac{n\pi y}{b}, \tag{18}$$

where m and n, respectively, denote the orders of vibration displacement in x and y directions.

We take one term of equation (18) for computation; i.e.,

$$w(x, y, t) = T_{mn}(t)\sin\frac{m\pi x}{a}\sin\frac{n\pi y}{b}. \tag{19}$$

Let $W_{mn}(x, y) = W(x, y) = W$ and $T_{mn}(t) = T(t) = T$.

The substitution of equation (19) into equation (9) yields

$$\frac{1}{E_1}\frac{\partial^4 \varphi}{\partial y^4} + \frac{1}{E_2}\frac{\partial^4 \varphi}{\partial x^4} = T^2(t)\frac{m^2n^2\pi^4}{a^2b^2}\left(\cos\frac{2m\pi x}{a} + \cos\frac{2n\pi y}{b}\right) + T(t)W(x, y)\left(k_{0x}\frac{n^2\pi^2}{b^2} + k_{0y}\frac{m^2\pi^2}{a^2}\right). \tag{20}$$

The stress function $\varphi(x, y, t)$ should satisfy the stress boundary condition (16), on the basic of the differential

Table 1: Mass and velocity of hailstone with different diameters.

Diameter (cm)	1.0	2.0	3.0	4.0	5.0	6.0
Mass (kg)	0.0005	0.0038	0.0127	0.0302	0.0589	0.1017
Mass difference		0.0033	0.0089	0.0175	0.0287	0.0428
Velocity (m/s)	16.12	21.38	25.22	28.36	31.06	35.74
Velocity squared difference		197.25	178.94	168.24	160.43	312.62

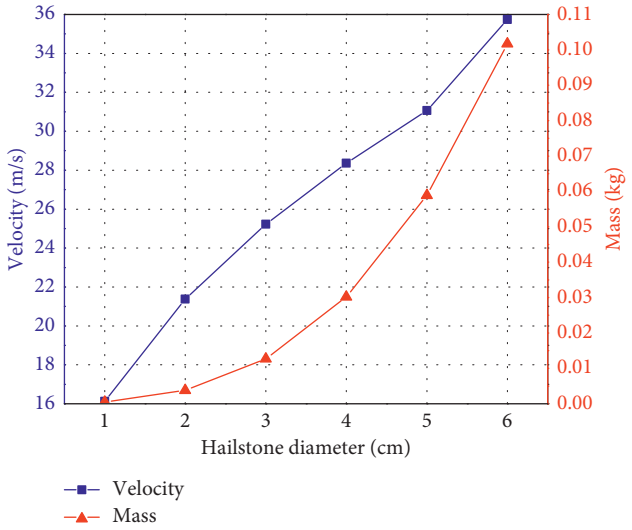

Figure 2: Mass and velocity of hailstone in different diameters.

equation theory. Therefore, the general solution of $\varphi(x, y, t)$ may be assumed as follows:

$$\varphi(x,y,t) = T^2(t)\left(\alpha\cos\frac{2m\pi x}{a} + \beta\cos\frac{2n\pi y}{b} + \gamma_1 x^3 + \gamma_2 x^2 + \gamma_3 x + \gamma_4 y^3 + \gamma_5 y^2 + \gamma_6 y + \gamma_7\right) + T(t)\sin\frac{m\pi x}{a}\sin\frac{n\pi y}{b}\lambda. \tag{21}$$

Let

$$\begin{cases} \varphi(x,y,t) = T^2(t)\Phi_1(x,y) + T(t)\Phi_2(x,y), \\ \Phi_1(x,y) = \alpha\cos\dfrac{2m\pi x}{a} + \beta\cos\dfrac{2n\pi y}{b} + \gamma_1 x^3 + \gamma_2 x^2 + \gamma_3 x + \gamma_4 y^3 + \gamma_5 y^2 + \gamma_6 y + \gamma_7, \\ \Phi_2(x,y) = \lambda\sin\dfrac{m\pi x}{a}\sin\dfrac{n\pi y}{b} = \lambda W(x,y). \end{cases} \tag{22}$$

The substitution of equation (21) into equation (16) yields

$$\begin{aligned} \alpha &= \frac{E_2 n^2 a^2}{32m^2 b^2}, \\ \beta &= \frac{E_1 m^2 b^2}{32n^2 a^2}, \\ \lambda &= \frac{k_{0x}(n\pi/b)^2 + k_{0y}(m\pi/a)^2}{\left((n\pi/b)^4/E_1\right) + \left((m\pi/a)^4/E_2\right)}, \\ \gamma_1 &= 0, \\ \gamma_2 &= \frac{\pi^2 E_2 n^2}{16b^2}, \\ \gamma_4 &= 0, \\ \gamma_5 &= \frac{\pi^2 E_1 m^2}{16a^2}, \end{aligned} \tag{23}$$

where γ_3, γ_6, and γ_7 are the arbitrary constant and can be set to zero to simplify the computation according to differential equations theory.

Then, the solution of $\varphi(x, y, t)$ is

$$\begin{cases} \varphi(x,y,t) = T^2(t)\Phi_1(x,y) + T(t)\Phi_2(x,y), \\ \Phi_1(x,y) = \dfrac{E_2 n^2 a^2}{32m^2 b^2}\cos\dfrac{2m\pi x}{a} + \dfrac{E_1 m^2 b^2}{32n^2 a^2}\cos\dfrac{2n\pi y}{b} + \dfrac{\pi^2 E_2 n^2}{16b^2}x^2 + \dfrac{\pi^2 E_1 m^2}{16a^2}y^2, \\ \Phi_2(x,y) = \dfrac{k_{0x}(n\pi/b)^2 + k_{0y}(m\pi/a)^2}{\left((n\pi/b)^4/E_1\right) + \left((m\pi/a)^4/E_2\right)}\sin\dfrac{m\pi x}{a}\sin\dfrac{n\pi y}{b}. \end{cases} \tag{24}$$

The substitution of equations (24), (19), and (10) into equation (8) yields

$$\rho_0 W T''(t) + cWT'(t) - \left(k_{0x}h\frac{\partial^2\Phi_2}{\partial y^2} + k_{0y}h\frac{\partial^2\Phi_2}{\partial x^2} + N_{0x}\frac{\partial^2 w}{\partial x^2} + N_{0y}\frac{\partial^2 w}{\partial y^2}\right)T(t) - \left(k_{0x}h\frac{\partial^2\Phi_1}{\partial y^2} + k_{0y}h\frac{\partial^2\Phi_1}{\partial x^2} + h\frac{\partial^2\Phi_2}{\partial y^2}\frac{\partial^2 w}{\partial x^2} + h\frac{\partial^2\Phi_2}{\partial x^2}\frac{\partial^2 w}{\partial y^2}\right)T^2(t) - \left(h\frac{\partial^2\Phi_1}{\partial y^2}\frac{\partial^2 w}{\partial x^2} + h\frac{\partial^2\Phi_1}{\partial x^2}\frac{\partial^2 w}{\partial y^2}\right)T^3(t) = F(t)\delta((x-x_0)(y-y_0)), \tag{25}$$

where $T'(t) = dT(t)/dt$ and $T''(t) = d^2T(t)/dt^2$.

By applying the Bubnov–Galerkin method [4], equation (25) can be transformed into

$$\begin{aligned}\iint_s \Bigg\{ & \rho_0 W T''(t) + cWT'(t) - \left(k_{0x} h \frac{\partial^2 \Phi_2}{\partial y^2} + k_{0y} h \frac{\partial^2 \Phi_2}{\partial x^2} \right. \\ & \left. + N_{0x} \frac{\partial^2 w}{\partial x^2} + N_{0y} \frac{\partial^2 w}{\partial y^2} \right) T(t) - \left(k_{0x} h \frac{\partial^2 \Phi_1}{\partial y^2} + k_{0y} h \frac{\partial^2 \Phi_1}{\partial x^2} \right. \\ & \left. + h \frac{\partial^2 \Phi_2}{\partial y^2} \frac{\partial^2 w}{\partial x^2} + h \frac{\partial^2 \Phi_2}{\partial x^2} \frac{\partial^2 w}{\partial y^2} \right) T^2(t) \\ & - \left(h \frac{\partial^2 \Phi_1}{\partial y^2} \frac{\partial^2 w}{\partial x^2} + h \frac{\partial^2 \Phi_1}{\partial x^2} \frac{\partial^2 w}{\partial y^2} \right) T^3(t) \Bigg\} W(x, y) dx\, dy \\ & = \iint_s F(t) \delta((x - x_0)(y - y_0)) W(x, y) dx\, dy, \end{aligned} \tag{26}$$

where

$$F(t) = -M \frac{\partial^2 w(x_0, y_0, t)}{\partial t^2} = -MW(x_0, y_0) T''(t). \tag{27}$$

Equation (26) can be simplified into a homogeneous differential equation as follows:

$$\begin{aligned} & T''(t) + \frac{B}{A - F} T'(t) + \frac{C}{A - F} T(t) + \frac{D}{A - F} T^2(t) \\ & \quad + \frac{E}{A - F} T^3(t) = 0, \end{aligned} \tag{28}$$

where

$$\begin{aligned} A &= \iint_S \rho_0 W^2 dx\, dy = \frac{ab}{4} \rho_0, \\ B &= \iint_S cW^2 dx\, dy = \frac{ab}{4} c, \\ C &= \iint_S -\left(k_{0x} h \frac{\partial^2 \Phi_2}{\partial y^2} + k_{0y} h \frac{\partial^2 \Phi_2}{\partial x^2} + N_{0x} \frac{\partial^2 w}{\partial x^2} + N_{0y} \frac{\partial^2 w}{\partial y^2} \right) W\, dx\, dy \\ &= \frac{m^2 \pi^2 b^2 \left(N_{0x} + h k_{0y} \lambda \right) + n^2 \pi^2 a^2 \left(N_{0y} + h k_{0x} \lambda \right)}{4ab}, \\ D &= \iint_S -\left(k_{0x} h \frac{\partial^2 \Phi_1}{\partial y^2} + k_{0y} h \frac{\partial^2 \Phi_1}{\partial x^2} + h \frac{\partial^2 \Phi_2}{\partial y^2} \frac{\partial^2 w}{\partial x^2} + h \frac{\partial^2 \Phi_2}{\partial x^2} \frac{\partial^2 w}{\partial y^2} \right) W\, dx\, dy, \\ E &= \iint_S -\left(h \frac{\partial^2 \Phi_1}{\partial y^2} \frac{\partial^2 w}{\partial x^2} + h \frac{\partial^2 \Phi_1}{\partial x^2} \frac{\partial^2 w}{\partial y^2} \right) W\, dx\, dy \\ &= h\pi^4 \frac{3E_1 m^4 b^4 + 3E_2 n^4 a^4}{64 a^3 b^3}, \\ F &= \iint_S F(t) \delta((x - x_0)(y - y_0)) W\, dx\, dy \\ &= -MW^2(x_0, y_0) = -M \sin^2 \frac{m\pi x_0}{a} \sin^2 \frac{n\pi y_0}{b}. \end{aligned} \tag{29}$$

The KBM perturbation method [13] is applied to solve equation (28). Assume the perturbation parameter is $\varepsilon = (h^2/ab) \ll 1$; then, equation (28) can be simplified by letting $x = x(t) = T(t)$ as follows:

$$\ddot{x} + \omega_0^2 x = \varepsilon \left(\alpha_1 x^3 + \alpha_2 x^2 + \alpha_3 \dot{x} \right), \tag{30}$$

where

$$\begin{aligned} {\omega_0}^2 &= \frac{C}{A - F}, \\ \alpha_1 &= \frac{-E}{\varepsilon (A - F)}, \\ \alpha_2 &= \frac{-D}{\varepsilon (A - F)}, \\ \alpha_3 &= \frac{-B}{\varepsilon (A - F)}, \\ \ddot{x} &= \frac{d^2 x}{dt^2}, \\ \dot{x} &= \frac{dx}{dt}. \end{aligned} \tag{31}$$

According to the perturbation method of KBM, let $f(x, \dot{x}) = \alpha_1 x^3 + \alpha_2 x^2 + \alpha_3 \dot{x}$ and the solution of equation (30) is

$$x = a \cos \psi. \tag{32}$$

In equation (32), a and ψ are determined by

$$\begin{aligned} \frac{da}{dt} &= -\frac{\varepsilon}{\omega_0} A_0(a), \\ \frac{d\psi}{dt} &= \omega_0 - \frac{\varepsilon}{a\omega_0} C_0(a), \end{aligned} \tag{33}$$

where

$$\begin{aligned} A_0(a) &= \frac{1}{2\pi} \int_0^{2\pi} \sin \varphi f(x, \dot{x}) d\psi = -\frac{1}{2} \alpha_3 a \omega_0, \\ C_0(a) &= \frac{1}{2\pi} \int_0^{2\pi} \cos \varphi f(x, \dot{x}) d\psi = \frac{3}{8} \alpha_1 a^3. \end{aligned} \tag{34}$$

The substitution of equaiton (34) into equation (33) yields

$$\begin{aligned} a &= De^{\varepsilon \alpha_3 t/2}, \\ \psi &= \left(\omega_0 - \frac{3\varepsilon \alpha_1 a^2}{8\omega_0} \right) t + \varphi_0, \end{aligned} \tag{35}$$

where D denotes the amplitude of vibration and φ_0 denotes the initial phase of vibration. They can be determined by the initial conditions of membrane vibration.

The substitution of equation (35) into equation (32) yields

$$x = x(t) = De^{\varepsilon \alpha_3 t/2} \cos \left(\left(\omega_0 - \frac{3\varepsilon \alpha_1 D^2 e^{\varepsilon \alpha_3 t}}{8\omega_0} \right) t + \varphi_0 \right). \tag{36}$$

Let

$$\omega = \omega_0 - \frac{3\varepsilon\alpha_1 D^2 e^{\varepsilon\alpha_3 t}}{8\omega_0}. \tag{37}$$

Equation (36) is the frequency function of vibration. According to equation (36), we can conclude that the amplitude of vibration and damping coefficient of structure have effect on the frequency of the nonlinear damped forced vibration of orthotropic saddle membrane structure.

The expression of initial conditions of membrane vibration can be obtained according to the principle of conservation of momentum:

$$x(t)|_{t=0} = 0, \tag{38}$$

$$\left.\frac{dx(t)}{dt}\right|_{t=0} = \frac{v_0}{\sin(m\pi x_0/a)\sin(n\pi y_0/b)}, \tag{39}$$

where $v_0 = Mv_H/(M + (4\rho_H ab/\pi^2))$; v_H is the initial velocity of hailstone; v_0 is the initial velocity of the system that consisted of hailstone and the membrane impact point; M is the mass of hailstone; ρ_H is the density of hailstone.

The substitution of equation (38) into equation (36) yields

$$x(0) = D\cos\varphi_0 = 0. \tag{40}$$

In equation (40), the amplitude of vibration is $D > 0$ and there will undoubtedly be $\cos\varphi_0 = 0$; therefore, $\varphi_0 = k\pi/2$, $(k = 1, 3, 5, \ldots)$. Taking $\varphi_0 = \pi/2$ and substituting it into equation (36) yields

$$x = x(t) = De^{\varepsilon\alpha_3 t/2}\cos\left(\left(\omega_0 - \frac{3\varepsilon\alpha_1 D^2 e^{\varepsilon\alpha_3 t}}{8\omega_0}\right)t + \frac{\pi}{2}\right). \tag{41}$$

The substitution of the first derivative of equation (41) into equation (39) yields

$$D\left(\frac{3\varepsilon\alpha_1 D^2}{8\omega_0} - \omega_0\right) = \frac{v_0}{\sin(m\pi x_0/a)\sin(n\pi y_0/b)}. \tag{42}$$

We solved equation (42) by applying the root formula of simple cubic equation and obtained the real root expression of amplitude:

$$\begin{aligned} D = {} & \frac{\sqrt[3]{4\sqrt{81v_0^2\alpha_1{}^4\varepsilon^4\omega_0{}^2\csc^2(m\pi x_0/a)\csc^2(n\pi y_0/b) - 32\alpha_1^3\varepsilon^3\omega_0^6} + 36v_0\omega_0\alpha_1^2\varepsilon^2\csc(m\pi x_0/a)\csc(n\pi y_0/b)}}{3\alpha_1\varepsilon} \\ & - \frac{\sqrt[3]{4\sqrt{81v_0^2\alpha_1{}^4\varepsilon^4\omega_0{}^2\csc^2(m\pi x_0/a)\csc^2(n\pi y_0/b) - 32\omega_0^6\alpha_1^3\varepsilon^3} - 36v_0\omega_0\alpha_1^2\varepsilon^2\csc(m\pi x_0/a)\csc(n\pi y_0/b)}}{3\alpha_1\varepsilon}, \end{aligned} \tag{43}$$

where

$$\begin{aligned} \omega_0 &= \sqrt{\frac{m^2\pi^2b^2\left(N_{0x} + h\lambda k_{0y}\right)}{a^2b^2\rho_0 + 4abM\sin^2(m\pi x_0/a)\sin^2(n\pi y_0/b)} + \frac{n^2\pi^2a^2\left(N_{0y} + h\lambda k_{0x}\right)}{a^2b^2\rho_0 + 4abM\sin^2(m\pi x_0/a)\sin^2(n\pi y_0/b)}}, \\ \lambda &= \frac{k_{0x}(n\pi/b)^2 + k_{0y}(m\pi/a)^2}{\left((n\pi/b)^4/E_1\right) + \left((m\pi/a)^4/E_2\right)}, \\ \alpha_1 &= \frac{-3\pi^4\left(E_1m^4b^4 + E_2n^4a^4\right)}{16a^3b^3h\rho_0 + 64a^2b^2hM\sin^2(m\pi x_0/a)\sin^2(n\pi y_0/b)}, \\ \alpha_3 &= \frac{-a^2b^2c}{ab\rho_0h^2 + 4h^2M\sin^2(m\pi x_0/a)\sin^2(n\pi y_0/b)}, \\ k_{0x} &= \frac{8f_2}{a^2}, \\ k_{0y} &= -\frac{8f_1}{b^2}, \\ v_0 &= \frac{Mv_H}{M + (4\rho_H ab/\pi^2)}, \\ \varepsilon &= \frac{h^2}{ab}. \end{aligned} \tag{44}$$

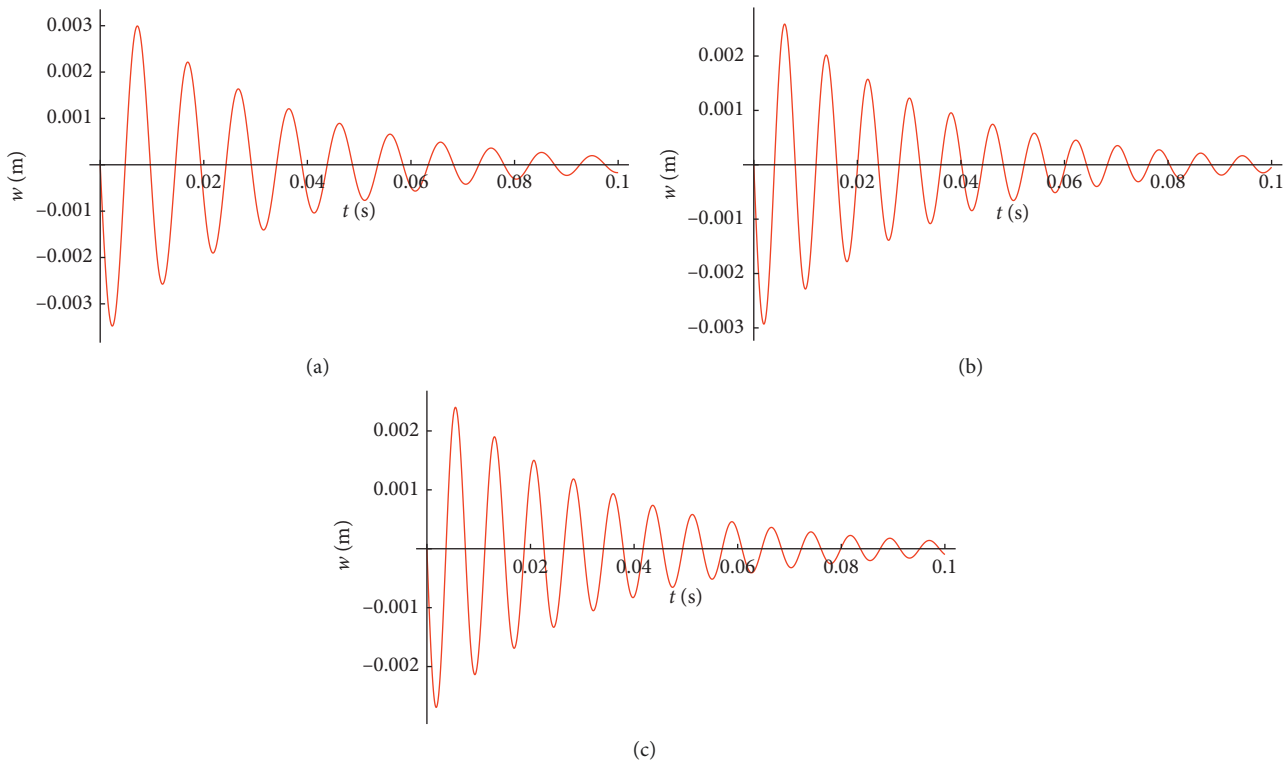

Figure 3: Time history curves of the first three orders of saddle membrane structure: (a) 1st order; (b) 2nd order; (c) 3rd order.

When $m+n=4i$, $(i=1,2,3,\ldots)$ and we can only obtain the amplitude of vibration $D>0$.

By substituting of equation (41) into equation (17), the displacement expression is obtained:

$$w(x,y,t)=\sum_{m=1}^{\infty}\sum_{n=1}^{\infty}\sin\frac{m\pi x}{a}\sin\frac{n\pi y}{b}De^{\varepsilon\alpha_3 t/2}\cdot\cos\left(\left(\omega_0-\frac{3\varepsilon\alpha_1D^2e^{\varepsilon\alpha_3 t}}{8\omega_0}\right)t+\frac{\pi}{2}\right),\tag{45}$$

where D is determined by equation (43). According to equation (45), we can obtain the mode of displacement of membrane surface.

Superposition of the initial surface function of saddle membrane structure equation (1) and its displacement expression equation (45), we can obtain the mode shape of the saddle membrane structure excited by impact of hailstone.

$$S=\frac{f_2(x-(a/2))^2}{(a/2)^2}-\frac{f_1(y-(b/2))^2}{(b/2)^2}+\sum_{m=1}^{\infty}\sum_{n=1}^{\infty}\sin\frac{m\pi x}{a}\cdot\sin\frac{n\pi y}{b}De^{\varepsilon\alpha_3 t/2}\cos\left(\left(\omega_0-\frac{3\varepsilon\alpha_1D^2e^{\varepsilon\alpha_3 t}}{8\omega_0}\right)t+\frac{\pi}{2}\right),\tag{46}$$

where S denotes the mode shape of the saddle membrane structure.

According to equation (46), we can obtain the modes of vibration and displacement time histories of the saddle membrane structures.

5. Analytical Examples

We take the orthotropic membrane that is widely used in practical engineering application as the analytical example: $E_1=1400$ MPa, $E_2=900$ MPa [16], the areal density of membrane $\rho_0=1.7\,\text{kg/m}^2$, the thickness $h=1.0$ mm, the length $a=1.0$ m, the width $b=1.0$ m, and the viscous damping $c=120$ Ns/m. We take the center point of membrane (i.e., $x_0=a/2$, $y_0=b/2$) as the impact point that is excited by hailstone.

5.1. Displacement Time Histories of Single Order. The arch-to-span ratio $f_1=f_2=1/10$, hailstone diameter $d=5.0$ cm, and pretension $N=1000$ N/m. According to equation (2), we can obtain $k_{0x}=0.8\,\text{m}^{-1}$ and $k_{0y}=-0.8\,\text{m}^{-1}$. According to equation (45), the impact point's first three-order vibration time histories are shown in Figure 3. From Figure 3, we can conclude that

(i) The maximum vibration amplitude decreases gradually with the increase of the vibration order (i.e., concluded from first order, second order to third order). The maximum vibration amplitude decreases the rate of first order to second order to 16.8% and second order to third order to 8.5%, and the decreases are nonlinear.

(ii) With the increasing of time, the maximum vibration amplitude of single order decreases gradually until it reaches zero.

Table 2: First three-order max. amplitude values (mm) of the impact point.

Arch-to-span ratio	Pretension (N/m)	Order	Hailstone diameter (cm)					
			1.0	2.0	3.0	4.0	5.0	6.0
1/10	1000	1st	0.016	0.170	0.674	1.783	3.743	7.098
		2nd	0.014	0.146	0.575	1.473	3.114	6.042
		3rd	0.013	0.140	0.556	1.468	2.849	5.144
	2000	1st	0.015	0.160	0.637	1.685	3.543	6.760
		2nd	0.013	0.135	0.534	1.415	2.994	5.818
		3rd	0.011	0.121	0.479	1.246	2.578	4.767
	3000	1st	0.014	0.152	0.604	1.600	3.370	6.461
		2nd	0.012	0.130	0.515	1.364	2.886	5.616
		3rd	0.010	0.108	0.429	1.132	2.368	4.446
	4000	1st	0.014	0.145	0.577	1.527	3.220	6.197
		2nd	0.012	0.125	0.497	1.318	2.789	5.433
		3rd	0.009	0.100	0.397	1.048	2.201	4.175
1/12	1000	1st	0.019	0.199	0.788	2.079	4.327	8.018
		2nd	0.016	0.165	0.655	1.734	3.656	7.026
		3rd	0.015	0.160	0.628	1.581	3.169	5.535
	2000	1st	0.017	0.184	0.729	1.927	4.030	7.562
		2nd	0.015	0.156	0.620	1.642	3.467	6.687
		3rd	0.012	0.131	0.519	1.366	2.817	5.102
	3000	1st	0.016	0.172	0.682	1.804	3.784	7.165
		2nd	0.014	0.149	0.590	1.564	3.303	6.391
		3rd	0.011	0.117	0.465	1.227	2.553	4.730
	4000	1st	0.015	0.162	0.643	1.701	3.577	6.819
		2nd	0.013	0.142	0.565	1.495	3.161	6.129
		3rd	0.010	0.107	0.425	1.123	2.349	4.416

5.2. Computation of Amplitude of Impact Point. The arch-to-span ratio are 1/12 and 1/10, the pretension levels increase from 1000 to 4000 N/m, and the hailstone diameters increase from 1.0 to 6.0 cm. According to equation (45), the max. amplitude of the impact point when $t = 0$ is obtained. The results of the first three orders are presented in Table 2.

Figures 4–6 show the results of Table 2. According to Table 2 and Figures 4–6, we can come to the following conclusions:

(i) When the arch-to-span ratio is 1/10 and the pretension level is 3000 N/m, the single-order maximum amplitude of the impact point decreases with respect to increasing vibration order; the single-order maximum amplitude of the impact point increases with respect to hailstone diameter increasing, and the increase is nonlinear (i.e., the increment of the maximum amplitude became smaller and smaller).

(ii) When the arch-to-span ratio is 1/10 and the hailstone diameter is 5.0 cm, the single-order maximum amplitude of impact point decreases with respect to the increasing pretensions and the decrement of the maximum amplitude became smaller and smaller. This reflects the nonlinearity of the of the membrane vibration.

(iii) When the pretension level is 3000 N/m and hailstone diameter is 5.0 cm, the impact point maximum amplitude of single order decreases with respect to increasing arch-to-span ratio and the decrease is nonlinear.

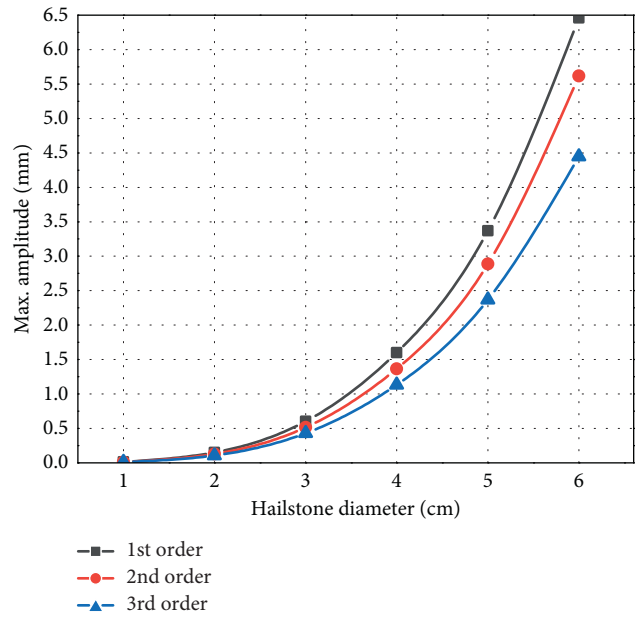

Figure 4: First three-order max. amplitude under impact of hailstone with different diameters when arch-to-span ratio is 1/10 and pretension level is 3000 N/m.

5.3. Total Displacement Time Histories. The arch-to-span ratio is 1/10, and the pretension level is 1000 N/m. According to equation (45), the total displacement time history of impact point is shown in Figure 7, when hailstone diameter is 5.0 cm.

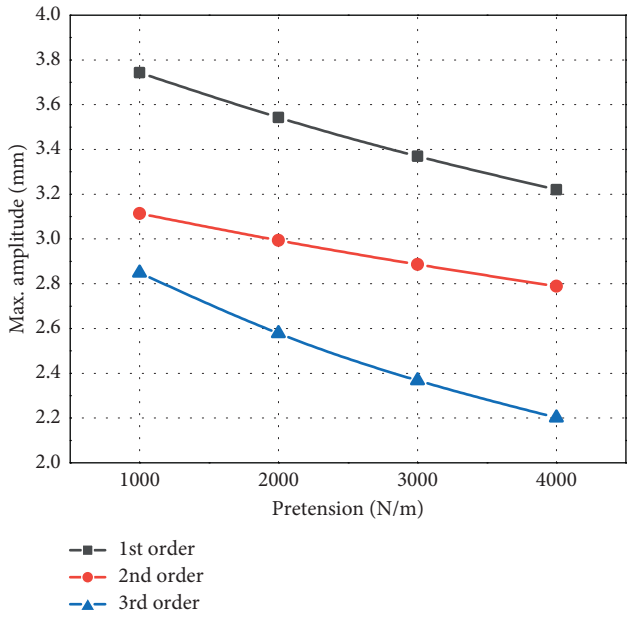

Figure 5: First three-order max. amplitude under different pretension levels when arch-to-span ratio is 1/10 and hailstone diameter is 5.0 cm.

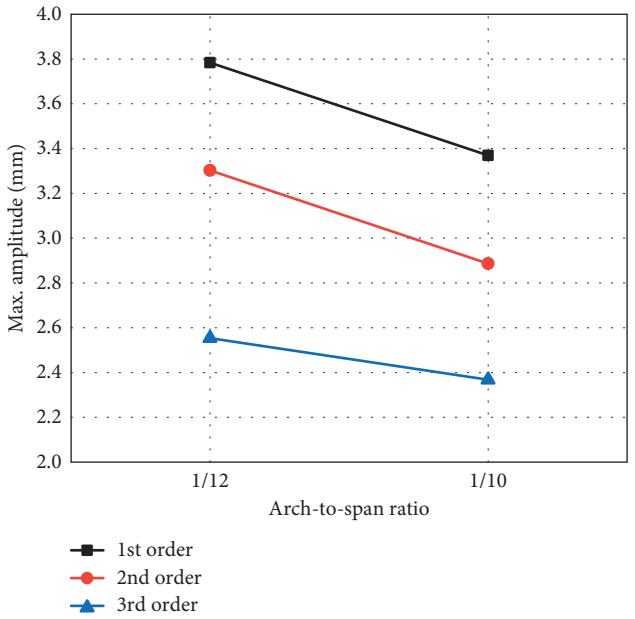

Figure 6: First three-order max. amplitude under different arch-to-span ratios when the pretension level is 3000 N/m and hailstone diameter is 5.0 cm.

From Figure 7, we can observe that the impact point did weaken the vibration; i.e., the amplitude rapidly increases to its maximum when the membrane is excited by hailstone. Soon afterwards, with the increase of time, the maximum amplitude decreases gradually until it reaches zero.

5.4. Computation of Total Displacement of Impact Point. The arch-to-span ratios are 1/12 and 1/10, the pretension levels increase from 1000 to 4000 N/m, and the hailstone

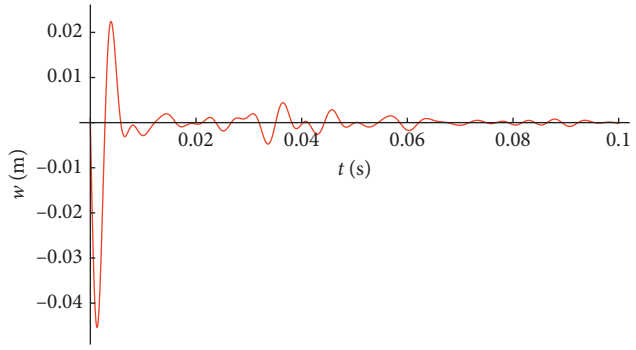

Figure 7: Total displacement time history curve of impact point.

diameters increase from 1.0 to 6.0 cm. According to equation (45), the total displacement values of the impact point are calculated and listed in Table 3.

Figures 8–10 show the results of Table 3. According to Table 3 and Figures 8–10, we can come to the following conclusions:

(i) The max. total displacement of the impact point increases with the increase of hailstone diameter. When the arch-to-span ratio is 1/10 and the pretension level is 3000 N/m and with the hailstone diameter increasing from 1.0 to 6.0 cm, the growth rates of maximum total displacement are 648%, 222%, 182%, 107%, and 83%, respectively. The growth rate of the max. total displacement became smaller and smaller.

(ii) As the membrane surface is subjected to effect of stress stiffening, the max. total displacement of impact point decreases with respect to increasing pretension levels. When arch-to-span ratio is 1/10 and the hailstone diameter is 6.0 cm, and with the pretension levels increasing from 1000 to 4000 N/m, the decrease rates of maximum total displacement are 8.3%, 8.1%, and 7.5%, respectively. The decrease rate of the max. total displacement became smaller and smaller. This reflects the nonlinearity of the membrane vibration.

(iii) The max. total displacement of impact point increases with the increase of arch-to-span ratio, and the increase is nonlinear.

5.5. Computation of Frequency

5.5.1. Hailstone Diameter. The arch-to-span ratio is 1/10, and the pretension level is 3000 N/m. The hailstone diameters increased from 1.0 to 6.0 cm. According to equation (37), the single-order frequency is affected by the hailstone diameter and time. The frequencies of the first three orders with different hailstone diameters and time instants are calculated and listed in Table 4.

Figures 11 and 12 show the results of Table 4. According to Table 4 and Figures 11 and 12, we can come to the following conclusions:

Table 3: Max. total displacement values (mm) of the impact point.

Arch-to-span ratio	Pretension (N/m)	Hailstone diameter (cm)					
		1.0	2.0	3.0	4.0	5.0	6.0
1/10	1000	0.31	2.22	7.36	19.04	37.46	63.06
	2000	0.24	1.82	6.16	16.15	32.88	58.25
	3000	0.21	1.57	5.05	14.25	29.47	53.87
	4000	0.18	1.41	4.73	12.89	25.05	50.11
1/12	1000	0.33	2.39	8.00	20.53	39.64	65.10
	2000	0.25	1.90	6.52	17.05	34.45	60.14
	3000	0.21	1.63	5.48	14.86	30.63	55.49
	4000	0.18	1.45	5.05	13.34	27.77	51.47

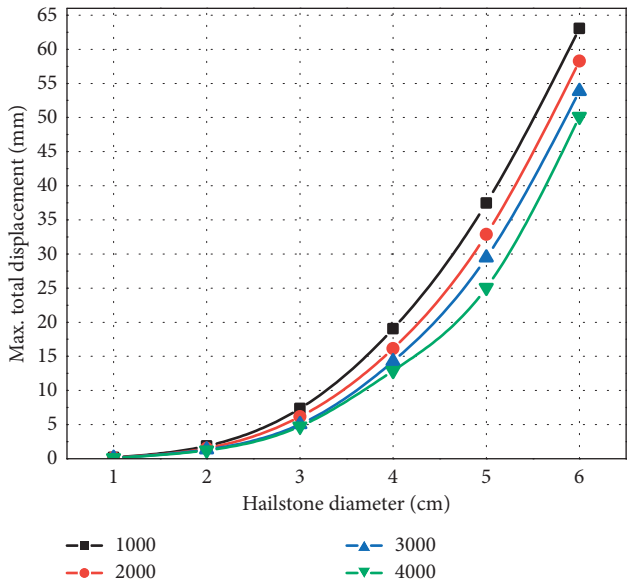

Figure 8: Max. total displacement curves of the impact point when arch-to-span ratio is 1/10 and the pretension levels increase from 1000 to 4000 N/m.

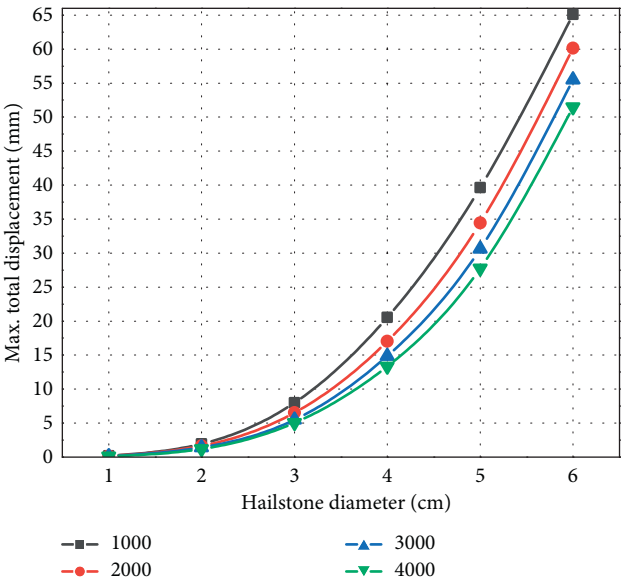

Figure 9: Total displacement curves of the impact point when arch-to-span ratio is 1/12 and the pretension levels increase from 1000 to 4000 N/m.

(i) In the case of the hail diameter being constant, the vibration frequencies increase with respect to the increasing vibration order. The frequencies of each order are maximum at $t = 0$ and gradually decrease to ω_0 with increase of time. This reflects the nonlinearity of the damped forced vibration of the membrane.

(ii) When $t = 0$, according to equation (37), the vibration frequency value is dependent on ω_0 and amplitude. Amplitudes of each order increase with the increase of hailstone diameter. This shows that the vibration frequency value of $t = 0$ decreases with respect to increasing hailstone diameter. But, the higher-order vibration (i.e., begin with the 3rd order) frequencies value of $t = 0$ increase when hailstone diameter increases from 5.0 to 6.0 cm. According to equation (43) and equation (38), in terms of the velocity and the mass of hailstone, the velocity has a higher-order (i.e., v^2) effect on vibration amplitude and frequency than the mass (i.e. m^{-1}), which is more significant in higher-order

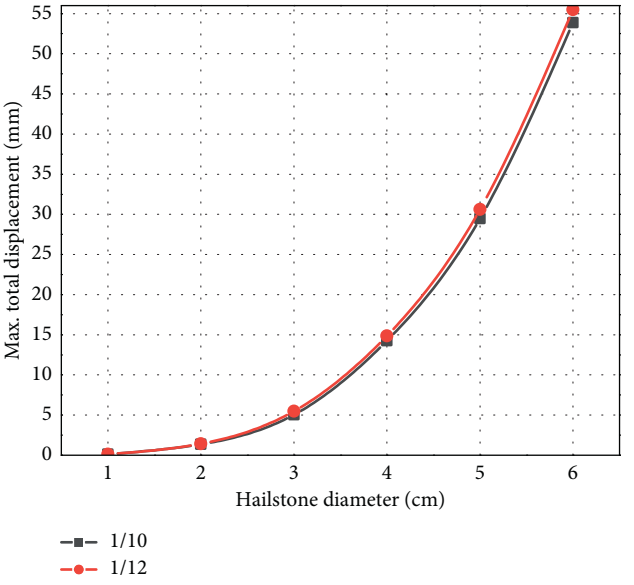

Figure 10: Total displacement curves of the impact point when the pretension level is 3000 N/m and arch-to-span ratio is 1/12 and 1/10.

Table 4: Frequencies (rad/s) under different hailstone diameters and time instants.

Order	Time (s)	Hailstone diameter (cm)					
		1.0	2.0	3.0	4.0	5.0	6.0
1st order	0.000	767.153	764.210	756.556	743.197	725.732	711.945
	0.005	767.153	764.206	756.494	742.780	724.029	706.369
	0.010	767.153	764.203	756.449	742.480	722.781	702.175
	0.050	767.153	764.197	756.347	741.767	719.633	690.749
	0.100	767.153	764.196	756.341	741.714	719.358	689.520
	$t \longrightarrow \infty$	767.153	764.196	756.340	741.712	719.345	689.445
2nd order	0.000	900.943	897.476	888.331	871.663	847.390	819.091
	0.005	900.943	897.475	888.306	871.495	846.699	816.760
	0.010	900.943	897.474	888.288	871.375	846.192	815.006
	0.050	900.943	897.471	888.248	871.088	844.914	810.228
	0.100	900.943	897.471	888.245	871.066	844.803	809.714
	$t \longrightarrow \infty$	900.943	897.471	888.245	871.066	844.797	809.683
3rd order	0.000	1081.37	1077.25	1066.77	1049.89	1032.55	1034.530
	0.005	1081.37	1077.24	1066.59	1048.66	1027.60	1018.990
	0.010	1081.37	1077.23	1066.45	1047.78	1023.97	1007.310
	0.050	1081.37	1077.21	1066.15	1045.68	1014.82	975.473
	0.100	1081.37	1077.21	1066.13	1045.52	1014.02	972.048
	$t \longrightarrow \infty$	1081.37	1077.21	1066.13	1045.51	1013.98	971.837
4th order	0.000	1105.53	1101.40	1092.06	1083.13	1094.00	1100.19
5th order	0.000	1184.02	1179.48	1167.68	1147.15	1120.50	1165.05
6th order	0.000	1190.68	1186.16	1174.99	1158.63	1147.61	1171.37
7th order	0.000	1395.95	1390.65	1377.50	1358.04	1344.08	1369.30

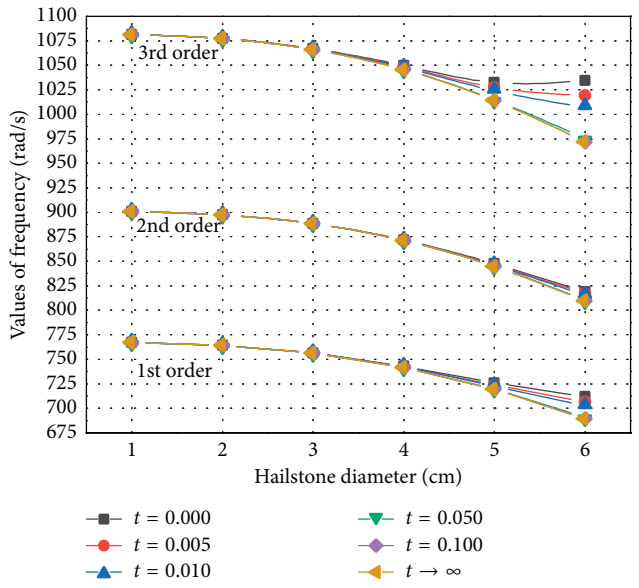

Figure 11: Frequencies (rad/s) under different hailstone diameters and time instants.

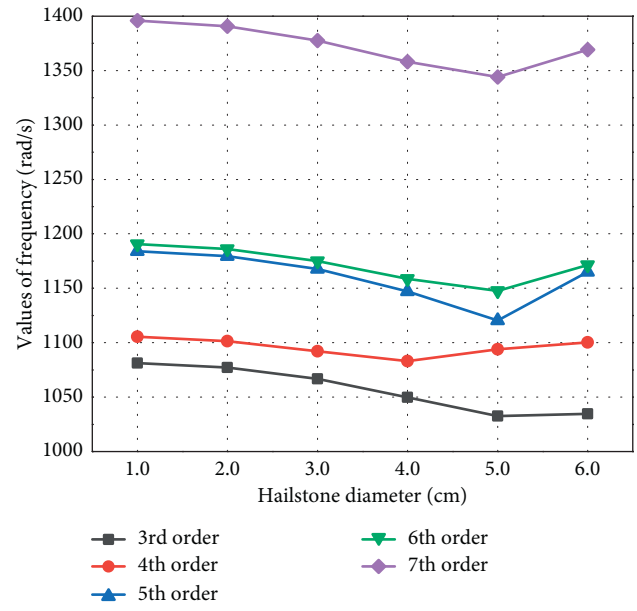

Figure 12: Frequencies (rad/s) under different hailstone diameters at $t = 0$.

vibration. When hailstone diameter increased from 5.0 to 6.0 cm, as shown in Table 1, the velocity squared difference increases rather than decreasing. Namely, the increase of velocity determines the increase of frequency as hailstone diameter increased from 5.0 to 6.0 cm. This is the reason why the higher-order vibration frequency value of $t = 0$ increases when hailstone diameter increased from 5.0 to 6.0 cm.

(iii) According to equation (37), when $t \longrightarrow \infty$, the vibration frequency value is only dependent on ω_0. The vibration frequency value of each order decreases with respect to increasing hailstone diameter.

5.5.2. Pretension Levels. The arch-to-span ratio is 1/10, and the hailstone diameter is 5.0 cm. The pretension levels increased from 1000 to 4000 N/m. Table 5 shows the first three-

Table 5: Frequencies (rad/s) under different pretensions and time instants.

Order	Time (s)	Pretension (N/m)			
		1000	2000	3000	4000
1st order	0.000	653.370	690.417	725.732	759.517
	0.005	651.026	688.436	724.029	758.034
	0.010	649.307	686.983	722.781	756.947
	0.050	644.972	683.319	719.633	754.205
	0.100	644.594	682.999	719.358	753.965
	$t \longrightarrow \infty$	644.576	682.984	719.345	753.954
2nd order	0.000	785.375	816.955	847.390	876.795
	0.005	784.506	816.183	846.699	876.171
	0.010	783.869	815.617	846.192	875.714
	0.050	782.262	814.190	844.914	874.561
	0.100	782.122	814.066	844.803	874.460
	$t \longrightarrow \infty$	782.115	814.060	844.797	874.455
3rd order	0.000	858.477	948.671	1032.55	1110.97
	0.005	849.685	942.243	1027.60	1107.02
	0.010	843.237	937.528	1023.97	1104.12
	0.050	826.978	925.641	1014.82	1096.81
	0.100	825.559	924.603	1014.02	1096.17
	$t \longrightarrow \infty$	825.492	924.554	1013.98	1096.14

order frequencies with different pretension levels and times, which are calculated according to equation (37).

Figure 13 shows the results of Table 5. According to Table 5 and Figure 13, we can conclude that the single-order frequencies increase with the increasing pretension levels. Moreover, the frequency increment of each order is bigger and bigger, so the increase is nonlinear.

5.5.3. Arch-to-Span Ratio. The pretension level is 3000 N/m, and the hailstone diameter is 5.0 cm. The arch-to-span ratio increased from 1/12 to 1/10. According to equation (37), the first three-order frequencies with different arch-to-span ratios and times are calculated and presented in Table 6.

Figure 14 shows the results of Table 6. According to Table 6 and Figure 14, we can conclude that the vibration frequencies of each order decrease with the decreasing arch-to-span ratio.

5.6. Mode Shape. The hailstone diameter is 6.0 cm, arch-to-span ratio is 1/10, pretension level is 1000 N/m, and time $t = 0.002$ s and 0.007 s. According to equation (46), the first three-order mode shapes are presented in Figures 15–20. By superimposing the first three-order mode shapes, the superposed mode shapes are obtained and shown in Figures 21 and 22. The coordinate dimension of Figures 15–22 is in meter.

By analyzing the mode shapes, we can conclude that the mode shape function equation (46) can be applied to calculate the single-order mode shapes and the total superposed mode shapes of the damped large nonlinear deflection vibration of orthotropic saddle membrane structures excited by hailstone impact load succinctly. In practical engineering vibration, the low-order mode shapes have a much bigger

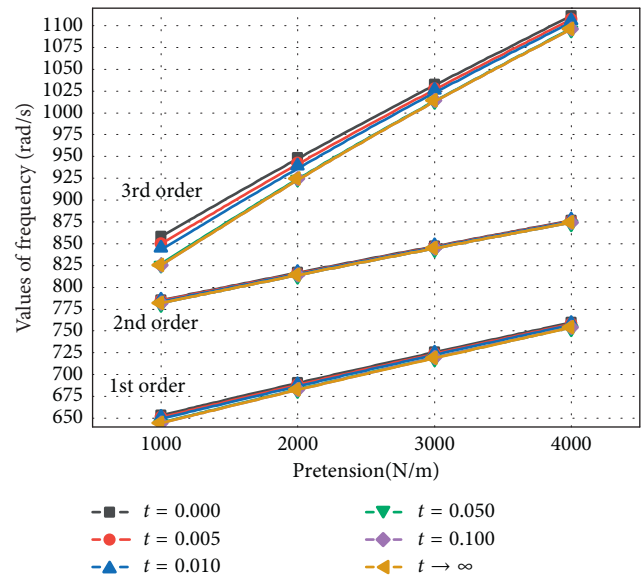

Figure 13: Frequencies (rad/s) under different pretension levels and time instants.

Table 6: Frequencies (rad/s) under different arch-to-span ratios and time instants.

Order	Time (s)	Arch-to-span ratio	
		1/10	1/12
1st order	0.000	725.732	646.338
	0.005	724.029	643.915
	0.010	722.781	642.138
	0.050	719.633	637.658
	0.100	719.358	637.267
	$t \longrightarrow \infty$	719.345	637.248
2nd order	0.000	847.390	740.343
	0.005	846.699	739.304
	0.010	846.192	738.543
	0.050	844.914	736.622
	0.100	844.803	736.454
	$t \longrightarrow \infty$	844.797	736.446
3rd order	0.000	1032.55	957.718
	0.005	1027.60	951.477
	0.010	1023.97	946.899
	0.050	1014.82	935.357
	0.100	1014.02	934.349
	$t \longrightarrow \infty$	1013.98	934.302

affect than the higher-order mode shapes, so we take the first three-order mode shapes into analysis.

5.7. Brief Summary

(1) The arch-to-span ratio is 1/10, and the pretension level is 3000 N/m. The hailstone diameters increased from 1.0 to 6.0 cm. We plot the first trough of time histories of the first-order vibration in Figure 23(a). From Figure 23(a), we can conclude that the hailstone diameter increase has a significant effect on the increase of amplitude and small effect on the decrease of frequency and increase of period.

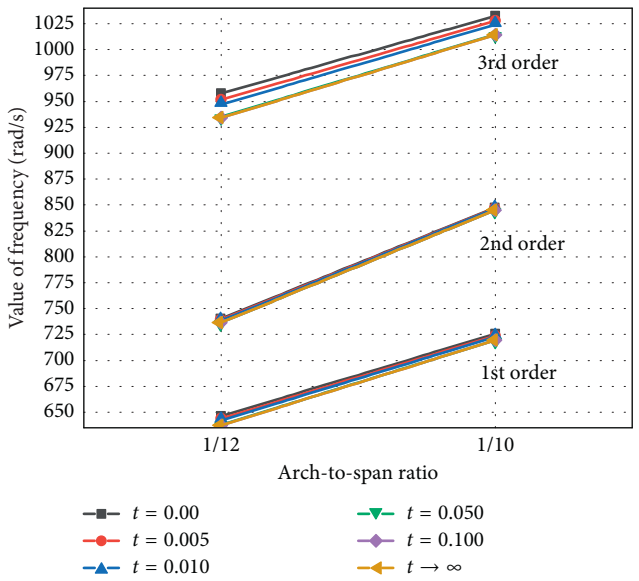

Figure 14: Frequencies (rad/s) with different arch-to-span ratios and time instants.

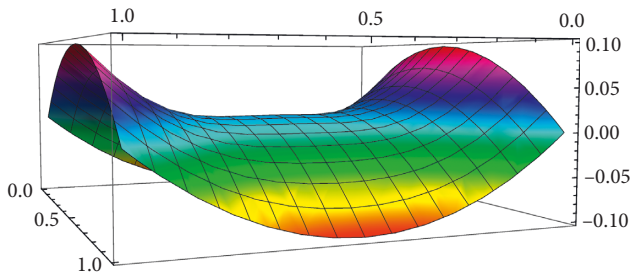

Figure 15: First order ($t = 0.002$ s).

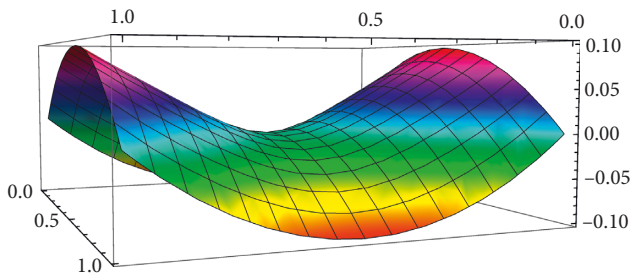

Figure 16: First order ($t = 0.007$ s).

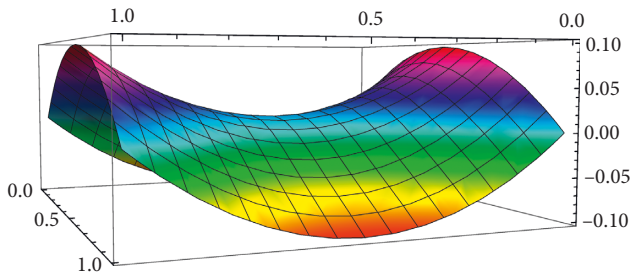

Figure 17: Second order ($t = 0.002$ s).

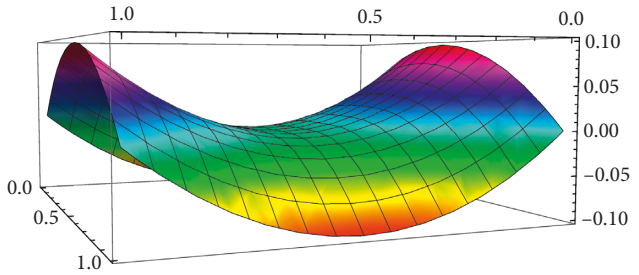

Figure 18: Second order ($t = 0.007$ s).

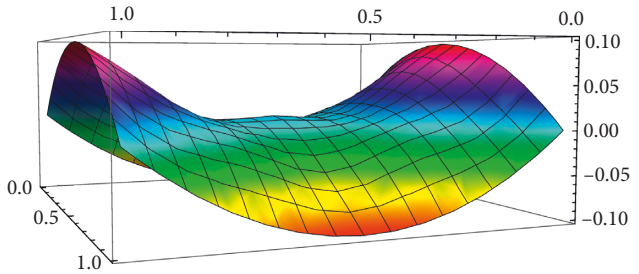

Figure 19: Third order ($t = 0.002$ s).

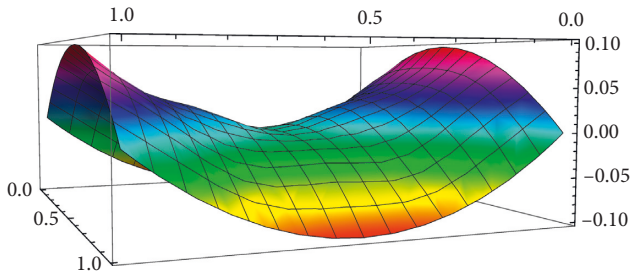

Figure 20: Third order ($t = 0.007$ s).

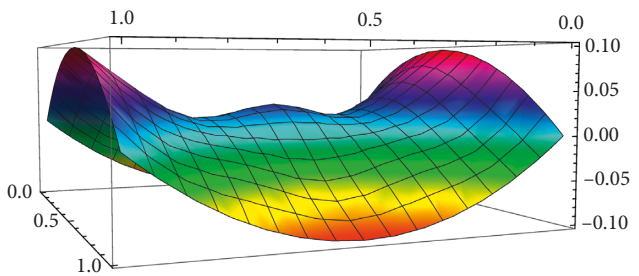

Figure 21: Superposing of the first three orders ($t = 0.002$ s).

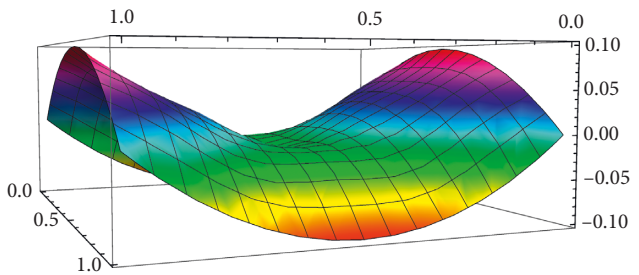

Figure 22: Superposing of the first three orders ($t = 0.007$ s).

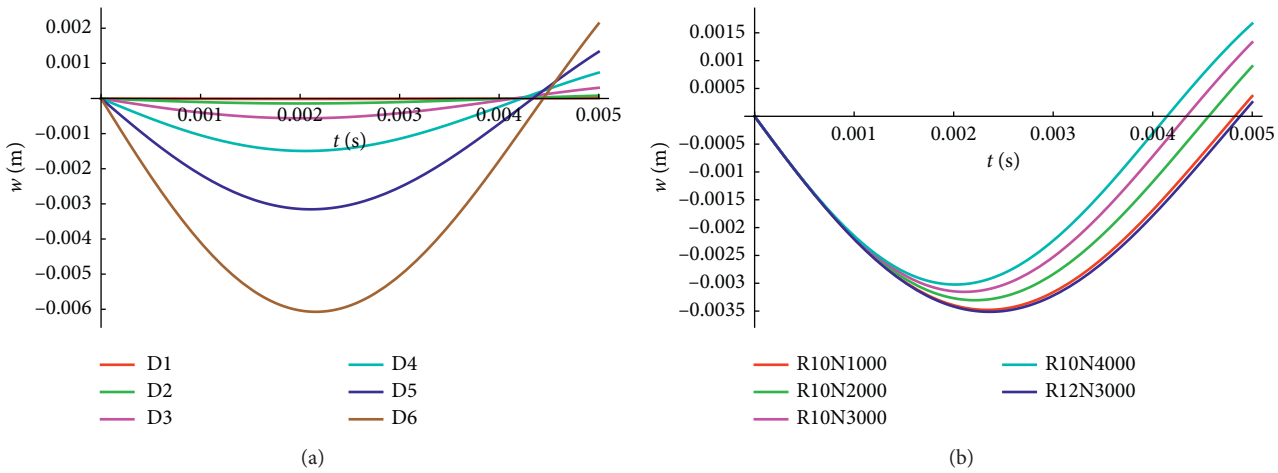

Figure 23: First trough of time histories of first-order vibration: (a) the arch-to-span ratio is 1/10, pretension level is 3000 N/m, and hailstone diameters increased from 1.0 to 6.0 cm (D1 to D6); (b) the hailstone diameter is 5.0 cm, the arch-to-span ratio are 1/12 and 1/10 (R10 and R12), and pretension levels increased from 1000 to 4000 N/m (N1000 to N4000).

(2) The hailstone diameter is 5.0 cm, and the arch-to-span ratios are 1/12 and 1/10. The pretension levels increased from 1000 to 4000 N/m. We plot the first trough of time histories of the first-order vibration in Figure 23(b). From Figure 23(b), we can conclude that the arch-to-span ratio decrease has a more significant effect on the increase of amplitude and the increase of period than that of decreasing pretension.

6. Numerical Simulation

In this section, we apply the universal explicit dynamics finite element analysis software ANSYS/LS-DYNA to simulate the process of hailstone impacting on the membrane based on the explicit-to-implicit sequential solution method. In implicit computation, Shell181 element is applied for the membrane and Solid185 element is applied for the hailstone. In explicit dynamic analysis, the elements will be converted to Shell163 and Solid164 element accordingly. We adopt a mapping triangle-shaped shell element to generate the mesh of the membrane surfaces and a mapping hexahedral-shaped solid element to generate the mesh for the hailstone. In ANSYS/LS-Dyna, the simulation results can converge better by refining the finite element mesh [33]. When hailstone diameter is 6.0 cm and arch-to-span ratio is 1/10, 5408 shell elements are generated with element size 2 cm and 4000 solid elements are generated with element size 0.5 cm, which satisfy the convergence accuracy. The results of the meshing are shown in Figures 24 and 25. The pretension load 1000 N/m is applied to the shell elements in implicit computation and converted to explicit dynamic analysis. In explicit dynamic analysis, the velocity according to Table 1 is applied to hailstone, automatic surface-to-surface contact is defined, and the corresponding parameter of the contact surface is set to describe the complex interaction among membranes in the large deformation contact and dynamic impact of

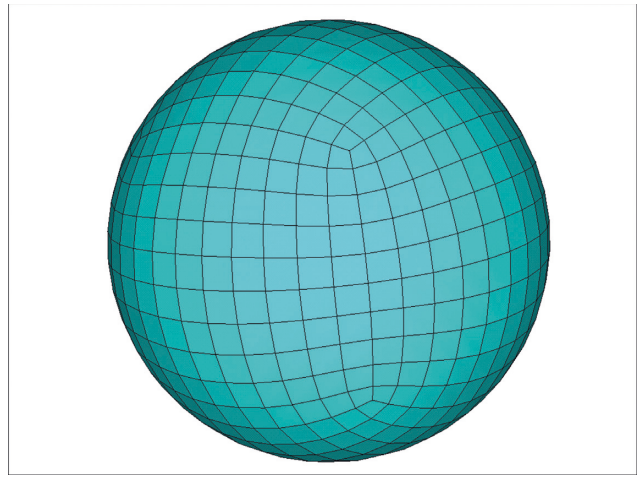

Figure 24: Solid elements of hailstone (diameter is 6.0 cm).

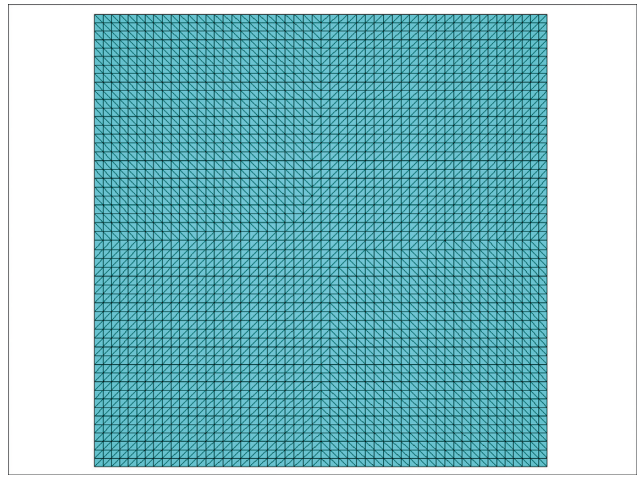

Figure 25: Shell of elements of membrane (arch-to-span ratio is 1/10).

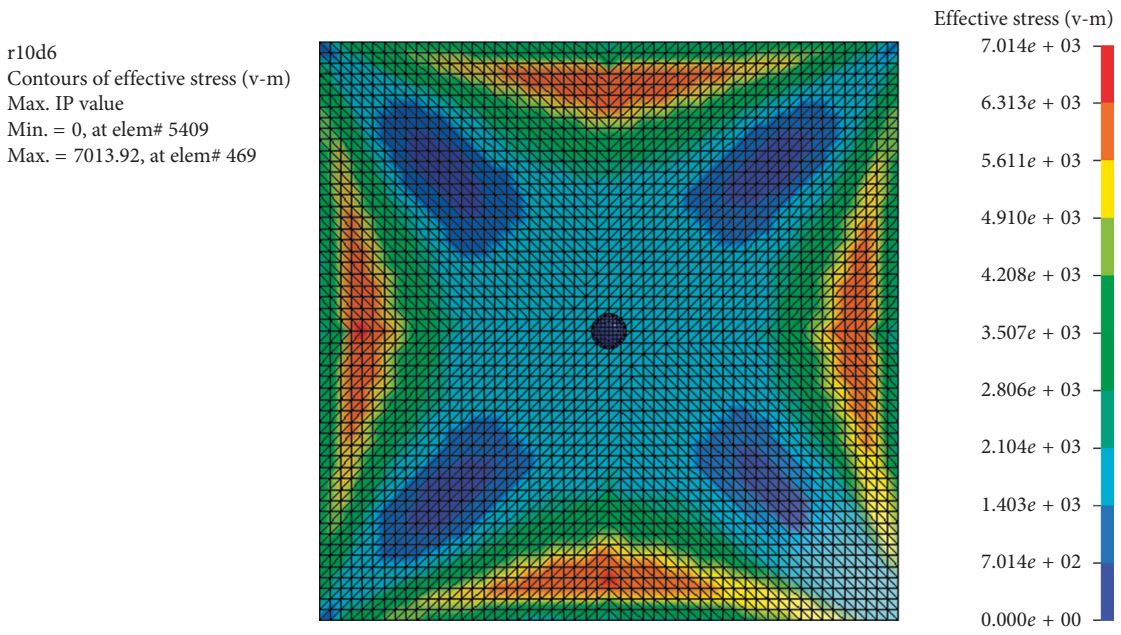

(a)

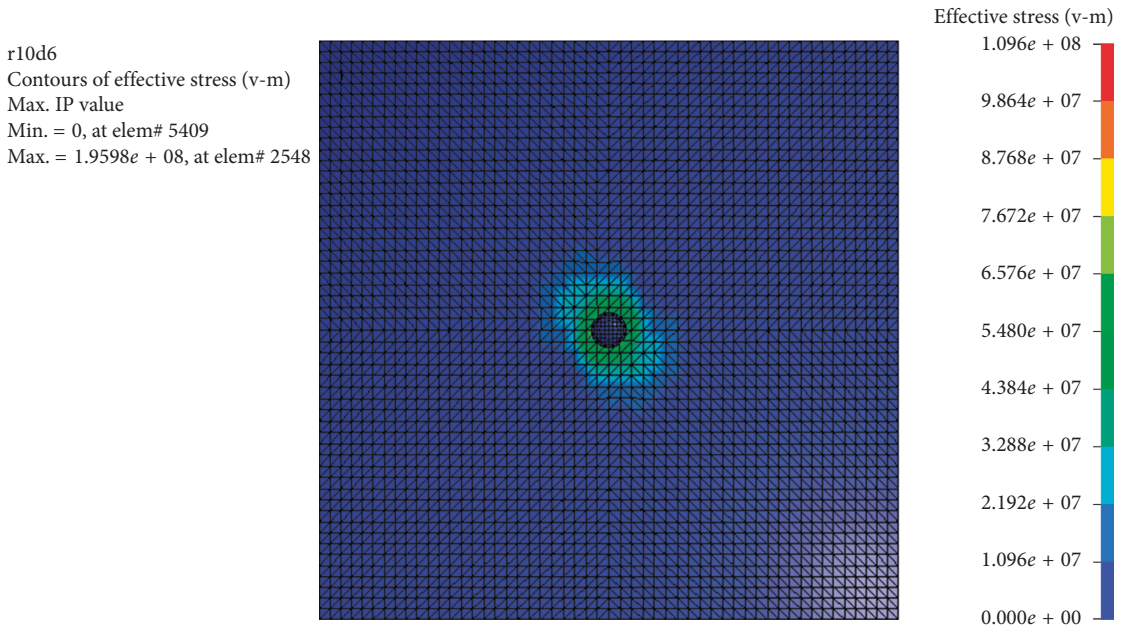

(b)

Figure 26: Continued.

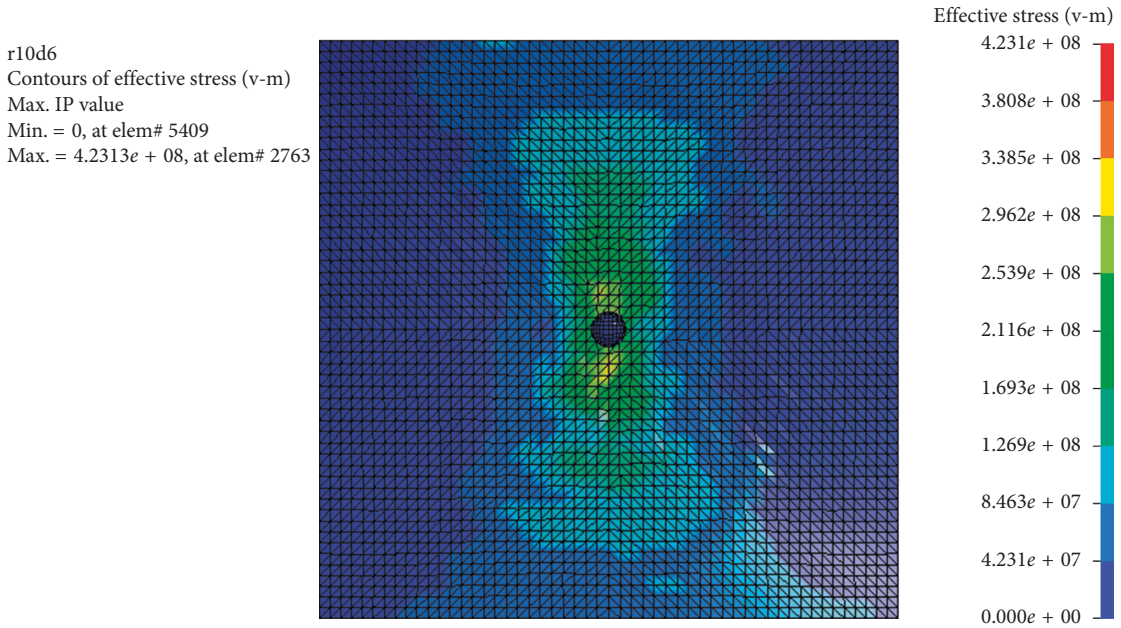

(c)

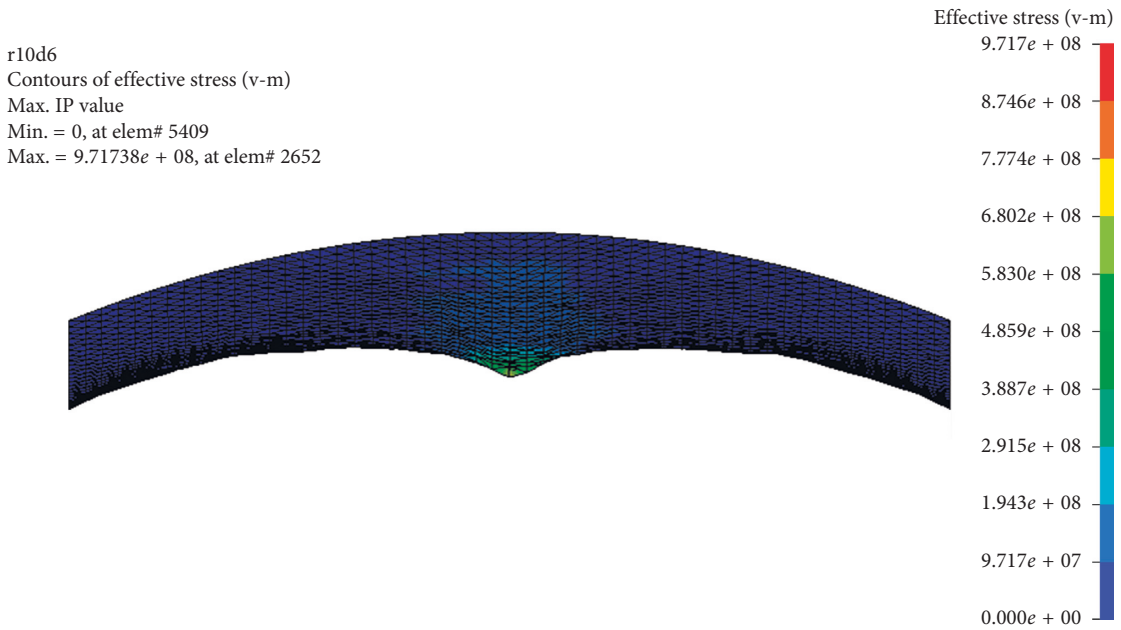

(d)

Figure 26: Continued.

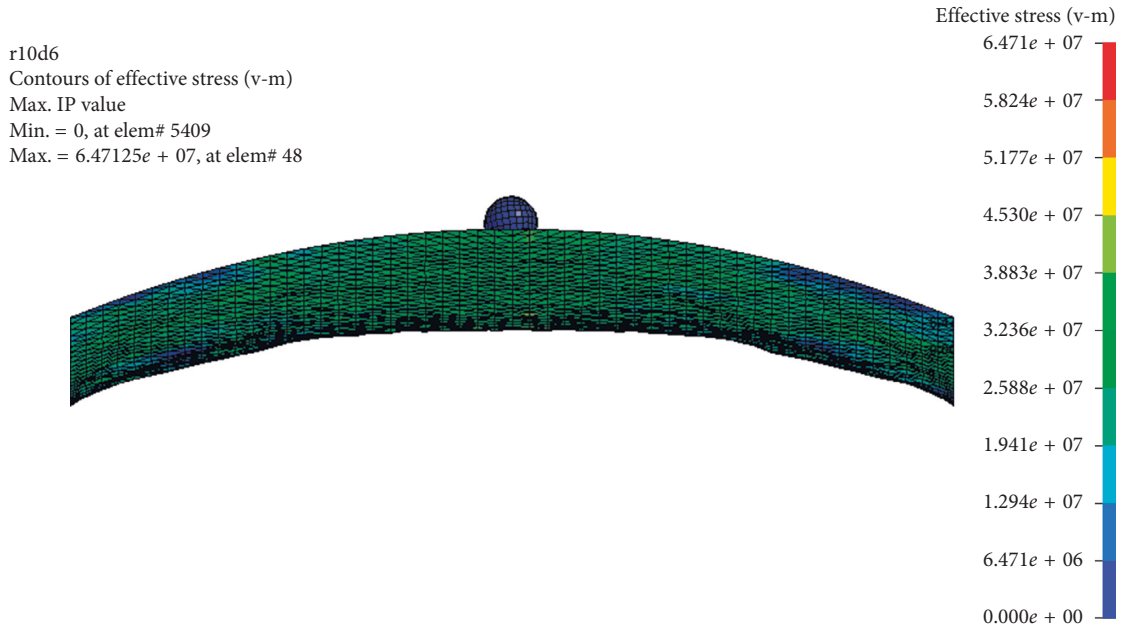

(e)

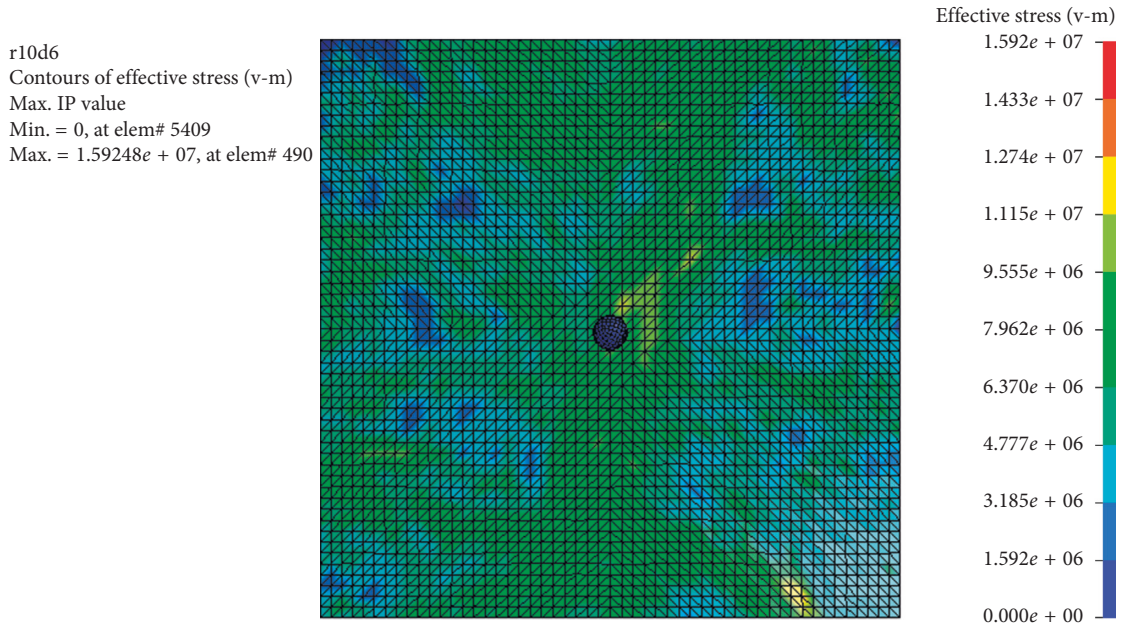

(f)

FIGURE 26: Dynamic response process of hailstone impacting on membrane surface: (a) when time = 0; (b) when hailstone impact on membrane surface; (c) and (d) when the displacement of the membrane is maximum; (e) and (f) when hailstone is bounced up.

hailstone. The Rayleigh damping coefficient is set to 0.05 that is recommended in explicit dynamic analysis.

Dynamic response process of hailstone impacting on membrane is shown in Figure 26. Time histories of the vertical displacement of impact point are shown in Figure 27. The following conclusions are drawn based on Figures 26 and 27:

(i) At the initial time ($t = 0$), the stress distribution in the membrane is more uniform. The maximum stress appears near the highest point and the lowest point and the minimum stress occurs near four corners. The mean stress in the membrane approximately is 1000 N/m.

(ii) The membrane material is elastic; it can only dissipate energy by deforming after being subjected to impact load. Therefore, when the hailstone impacted the membrane surface, most of the energy of hailstone is converted into the membrane strain

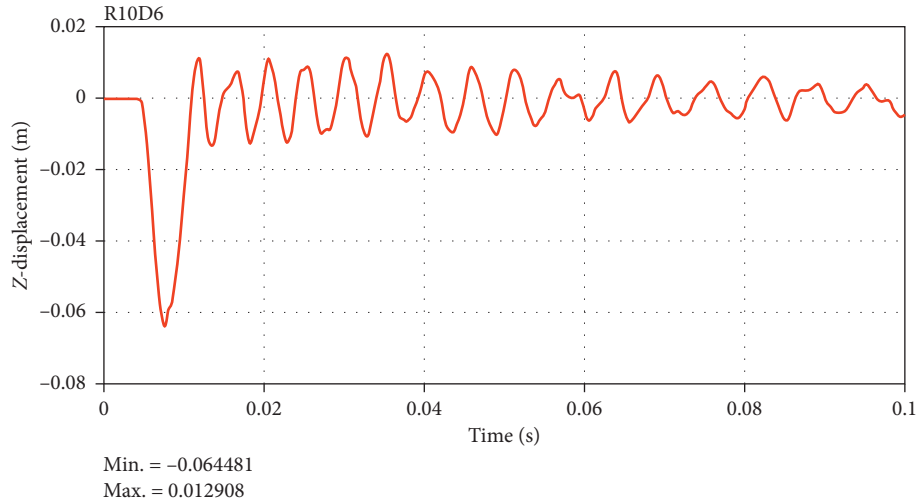

Figure 27: Time histories of the vertical displacement of impact point.

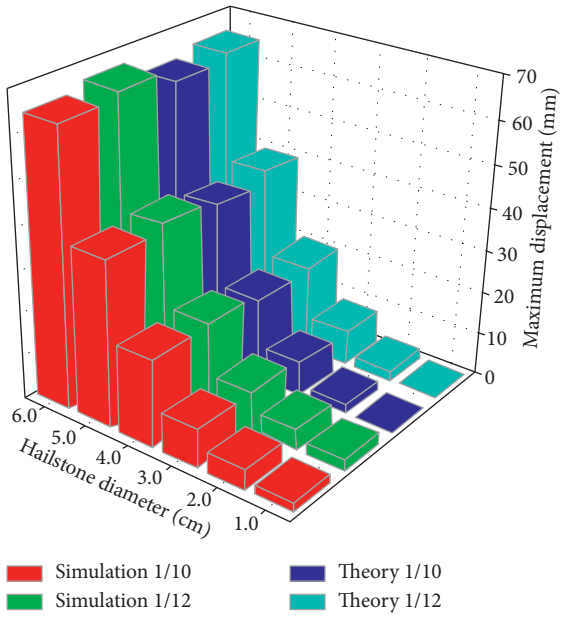

Figure 28: Comparison of impact point maximum displacement results between numerical simulations and theoretical solutions.

energy and the kinetic energy of the vibration [12], which results in the rapid increment of vertical displacement of the impact point. At the same time, the stress concentration occurs in the impact area and the membrane stress diffuses from the impact point to the two high points.

(iii) When the displacement of impact point is maximized, because of the pretension, the hailstone is rebounded up from the membrane and the membrane begins to vibrate freely. Subsequently, the displacement of the membrane attenuates gradually, and the vibration energy wave diffuses from the center to all around but rebounds at the boundary of membrane. This is the reason why the membrane stress exhibited irregularity.

7. Comparison and Analysis of Numerical Simulation and Theoretical Solution

The comparison of numerical simulation results and the theoretical results shows that the simulation results tally with the actual theoretical situation.

Figure 28 shows the results of Table 7. According to Table 7 and Figure 28, we can come to the following conclusions:

(i) The nonlinear dynamic response law of orthotropic saddle membrane structures excited by hailstone impact load which reflected in the numerical simulation results is consistent with the theoretical ones.

(ii) We neglected the dead load of membrane in the theoretical calculation. As a result of this, the theoretical results are slightly smaller (the maximum difference is less than 2.63 mm) than those of numerical simulation. The dead load of membrane is much more than the impact load of a hailstone when the diameters of hailstone are low; this is the main reason why the relative errors of simulation and theory are high at low hailstone diameters.

(iii) The theoretical calculation results basically fit the numerical simulation results, implying that our methods have been successful.

8. Conclusions

In this paper, the approximate formulas of hailstone terminal velocity were substituted into the governing equations of the large deflection nonlinear damped vibration of orthotropic saddle membrane structures excited by impact load. And, solving the governing equations by applying the Bubnov–Galerkin method and the method of KBM perturbation, the approximate theoretical solution of the frequency function and displacement function of the large deflection nonlinear damped vibration of saddle membrane

Table 7: Comparison of impact point maximum displacement results (mm) between numerical simulation and theoretical solution.

Results	Arch-to-span ratio	Pretension (N/m)	Hailstone diameter (cm)					
			1.0	2.0	3.0	4.0	5.0	6.0
Simulation	1/10	1000	1.77	4.69	9.18	20.48	38.90	64.48
Theory	1/10	1000	0.31	2.22	7.36	19.04	37.46	63.06
Relative error			82%	53%	20%	7%	4%	2%
Simulation	1/12	1000	2.73	5.02	9.42	20.97	40.14	66.53
Theory	1/12	1000	0.33	2.39	8.00	20.53	39.64	65.10
Relative error			88%	52%	15%	2%	1%	2%

structures with four edges simply supported excited by hailstone impact was obtained.

The analytical examples proved that the mode shape function equation (46) can be applied to calculate the single-order mode shapes and the total superposed mode shapes of the damped large nonlinear deflection vibration of orthotropic saddle membrane structures excited by hailstone impact load succinctly. In addition, we compare and analyze the results of vibration frequency, amplitude, time histories, and total displacement of membrane structures with different pretensions and arch-to-span ratios under the impact of different size hailstones, and the following conclusions can be drawn:

(i) The increasing hailstone diameter has a significant effect on the increase of amplitude and small effect on the decrease of frequency and increase of period

(ii) The decreasing arch-to-span ratio has a more significant effect on the increase of amplitude and the increase of period than that of decreasing pretension

The correctness of the analytical theory is verified by comparing with the results of numerical simulation. In addition, the results of this paper can be applied in computation for the vibration control and dynamic design of practical spatial membrane structure under impact load. Therefore, we put forward some suggestions for the vibration control and dynamic design of practical spatial membrane structures:

(i) In the preliminary design phase, the membrane structure with high arch-to-span ratio should be adopted as far as possible for a strong resistance to external load and vibration

(ii) After the arch-to-span ratio of membrane structure was determined, increasing the pretension helps resist external load and vibration control

Data Availability

The data used to support the findings of this study are available from the corresponding author upon request.

Conflicts of Interest

The authors declare that they have no conflicts of interest.

Acknowledgments

This work was supported by the National Natural Science Foundation of China (Project Numbers 51608060, 51678168, and 51878586), the Natural Science Foundation of Guangdong Province (Project Number 2017A030313267), and the Science and Technology Plan of Guangzhou City (Project Number 201607010107).

References

[1] K. Ando, A. Ishii, T. Suzuki, K. Masuda, and Y. Saito, "Design and construction of a double membrane air-supported structure," *Engineering Structures*, vol. 21, no. 8, pp. 786–794, 1999.

[2] P. D. Gosling, B. N. Bridgens, A. Albrecht et al., "Analysis and design of membrane structures: results of a round robin exercise," *Engineering Structures*, vol. 48, pp. 313–328, 2013.

[3] J. Gade, R. Kemmler, M. Drass, and J. Schneider, "Enhancement of a meso-scale material model for nonlinear elastic finite element computations of plain-woven fabric membrane structures," *Engineering Structures*, vol. 177, pp. 668–681, 2018.

[4] Y. Tang and T. Li, "Equivalent-force density method as a shape-finding tool for cable-membrane structures," *Engineering Structures*, vol. 151, pp. 11–19, 2017.

[5] C. Shin, J. Chung, and W. Kim, "Dynamic characteristics of the out-of-plane vibration for an axially moving membrane," *Journal of Sound and Vibration*, vol. 286, no. 4-5, pp. 1019–1031, 2005.

[6] C. Shin, W. Kim, and J. Chung, "Free in-plane vibration of an axially moving membrane," *Journal of Sound and Vibration*, vol. 272, no. 1-2, pp. 137–154, 2004.

[7] J. Pan and M. Gu, "Geometric nonlinear effect to square tensioned membrane's free vibration," *Journal of Tongji University Natural Science*, vol. 35, pp. 1450–1454, 2007.

[8] Z. L. Zheng, C. J. Liu, X. T. He, and S. L. Chen, "Free vibration analysis of rectangular orthotropic membranes in large deflection," *Mathematical Problems in Engineering*, vol. 2009, Article ID 634362, 9 pages, 2009.

[9] C. J. Liu, Z. L. Zheng, X. T. He et al., "L-P perturbation solution of nonlinear free vibration of prestressed orthotropic membrane in large amplitude," *Mathematical Problems in Engineering*, vol. 2010, Article ID 561364, 17 pages, 2010.

[10] D. Li, Z. L. Zheng, and M. D. Todd, "Nonlinear vibration of orthotropic rectangular membrane structures including modal coupling," *Journal of Applied Mechanics-Transactions of the ASME*, vol. 85, no. 6, article 061004, 2018.

[11] P. B. Gonçalves, R. M. Soares, and D. Pamplona, "Nonlinear vibrations of a radially stretched circular hyperelastic membrane," *Journal of Sound and Vibration*, vol. 327, no. 1-2, pp. 231–248, 2009.

[12] Z. L. Zheng, W. J. Song, C. J. Liu, X. T. He, J. Y. Sun, and Y. P. Xu, "Study on dynamic response of rectangular orthotropic membranes under impact loading," *Journal of*

Adhesion Science and Technology, vol. 26, no. 10-11, pp. 1467–1479, 2012.

[13] C. J. Liu, Z. L. Zheng, J. Long, J. J. Guo, and K. Wu, "Dynamic analysis for nonlinear vibration of prestressed orthotropic membranes with viscous damping," *International Journal of Structural Stability and Dynamics*, vol. 13, no. 2, article 1350018, 2013.

[14] Z. L. Zheng, C. Y. Liu, D. Li, and T. Zhang, "Dynamic response of orthotropic membrane structure under impact load based on multiple scale perturbation method," *Latin American Journal of Solids and Structures*, vol. 14, no. 8, pp. 1490–1505, 2017.

[15] Z. L. Zheng, C. J. Liu, W. C. Gong et al., "A new method—ejection method for nondestructive online monitoring of the pretension of building membrane structure," *Structural Control and Health Monitoring*, vol. 20, no. 4, pp. 445–464, 2013.

[16] C. J. Liu, Z. L. Zheng, X. Y. Yang, and H. Zhao, "Nonlinear damped vibration of pre-stressed orthotropic membrane structure under impact loading," *International Journal of Structural Stability and Dynamics*, vol. 14, no. 1, article 1350055, 2014.

[17] C. Liu, Z. Zheng, and X. Yang, "Analytical and numerical studies on the nonlinear dynamic response of orthotropic membranes under impact load," *Earthquake Engineering and Engineering Vibration*, vol. 15, no. 4, pp. 657–672, 2016.

[18] Z. L. Zheng, F. M. Lu, X. T. He, J. Y. Sun, C. X. Xie, and C. He, "Large displacement analysis of rectangular orthotropic membranes under stochastic impact loading," *International Journal of Structural Stability and Dynamics*, vol. 16, no. 1, article 1640007, 2016.

[19] D. Li, Z. L. Zheng, R. Yang, and P. Zhang, "Analytical solutions for stochastic vibration of orthotropic membrane under random impact load," *Materials*, vol. 11, no. 7, p. 1231, 2018.

[20] D. Li, Z. Zheng, Y. Tian, J. Sun, X. He, and Y. Lu, "Stochastic nonlinear vibration and reliability of orthotropic membrane structure under impact load," *Thin-Walled Structures*, vol. 119, pp. 247–255, 2017.

[21] D. Li, Z.-L. Zheng, C.-Y. Liu et al., "Dynamic response of rectangular prestressed membrane subjected to uniform impact load," *Archives of Civil and Mechanical Engineering*, vol. 17, no. 3, pp. 586–598, 2017.

[22] Q. S. Yang and R. X. Liu, "On aerodynamic stability of membrane structures," *Engineering Mechanics*, vol. 23, no. 9, pp. 18–29, 2006.

[23] Q. X. Li and B. N. Sun, "Wind-induced aerodynamic instability for closed membrane roofs," *Journal of Vibration Engineering*, vol. 19, pp. 346–353, 2006.

[24] M. Lazzari, M. Majowiecki, R. V. Vitaliani, and A. V. Saetta, "Nonlinear F.E. analysis of Montreal Olympic Stadium roof under natural loading conditions," *Engineering Structures*, vol. 31, no. 1, pp. 16–31, 2009.

[25] F. Rizzo, P. D'Asdia, M. Lazzari, and L. Procino, "Wind action evaluation on tension roofs of hyperbolic paraboloid shape," *Engineering Structures*, vol. 33, no. 2, pp. 445–461, 2011.

[26] F. Rizzo and V. Sepe, "Static loads to simulate dynamic effects of wind on hyperbolic paraboloid roofs with square plan," *Journal of Wind Engineering and Industrial Aerodynamics*, vol. 137, pp. 46–57, 2015.

[27] Y. Wu, Z.-Q. Chen, and X.-Y. Sun, "Research on the wind-induced aero-elastic response of closed-type saddle-shaped tensioned membrane models," *Journal of Zhejiang University-Science A*, vol. 16, no. 8, pp. 656–668, 2015.

[28] Y. P. Xu, Z. L. Zheng, C. J. Liu, K. Wu, and W. J. Song, "Aerodynamic stability analysis of geometrically nonlinear orthotropic membrane structure with hyperbolic paraboloid in sag direction," *Wind and Structures*, vol. 26, pp. 355–367, 2018.

[29] Y.-P. Xu, Z.-L. Zheng, C.-J. Liu, W.-J. Song, and J. Long, "Aerodynamic stability analysis of geometrically nonlinear orthotropic membrane structure with hyperbolic paraboloid," *Journal of Engineering Mechanics*, vol. 137, no. 11, pp. 759–768, 2011.

[30] C. Liu, X. Deng, and Z. Zheng, "Nonlinear wind-induced aerodynamic stability of orthotropic saddle membrane structures," *Journal of Wind Engineering and Industrial Aerodynamics*, vol. 164, pp. 119–127, 2017.

[31] W. Cui, L. Zhang, and H. Zhang, "The saddle membrane structure response analysis under the simultaneous actions of wind and rain based on multiphase flow theory," *Industrial Construction*, vol. 48, pp. 60–64, 2018.

[32] H. Chia-Liu, "Approximate formulas of hailstone drag coefficients and its terminal velocity," *Journal of Lanzhou University*, vol. 1, pp. 90–103, 1978.

[33] S. C. Her and Y. C. Liang, "The finite element analysis of composite laminates and shell structures subjected to low velocity impact," *Composite Structures*, vol. 66, no. 1–4, pp. 277–285, 2004.